MATHEMATICS OF COMPUTATION
Volume 88, Number 315, January 2019, Pages 237–271
http://dx.doi.org/10.1090/mcom/3334
Article electronically published on April 10, 2018

A NONCONFORMING CROUZEIX-RAVIART TYPE FINITE ELEMENT ON POLYGONAL MESHES

YANQIU WANG

Abstract. A nonconforming lowest order Crouzeix-Raviart type finite element, based on the generalized barycentric coordinates, is constructed on general polygonal (convex or nonconvex) meshes. We reveal a fundamental difference of the Crouzeix-Raviart type degrees of freedom between polygons with odd and even number of vertices, which results in slightly different local constructions of finite elements on these two types of polygons. Because of this, the topological structure of connected regions consisting of polygons with even number of vertices plays an essential role in understanding the global finite element space. To analyze such a topological structure, a new technical tool using the concept of cochain complex and cohomology is developed. Despite the seemingly complicated theoretical analysis, implementation of the element is straightforward. The nonconforming finite element method has optimal a priori error estimates. Proof and supporting numerical results are presented.

1. Introduction

The Crouzeix-Raviart nonconforming finite element [9] has been widely used and extensively studied on simplicial meshes. It is useful in constructing stable mixed discretizations for Stokes/Navier-Stokes equations and locking-free discretizations for elasticity problems, and thus has attracted the attention of many researchers. A good survey [4] of this element is given by Brenner in 2015, where readers may find references to an abundant literature on the topic.

Different from the case of simplicial meshes, extension of the nonconforming element to quadrilateral/hexahedral meshes is less straightforward. A direct application of Crouzeix and Raviart's original idea to quadrilateral/hexahedron does not produce unisolvent degrees of freedom. Efforts to seek alternative solutions include: Han's early work [21], Rannacher and Turek's rotated Q_1 element [36], the Douglas-Santos-Sheen-Ye (DSSY) element [7,14], Lin, Tobiska, and Zhou's enriched rotated Q_1 element [30], Park and Sheen's P_1 nonconforming element [35], Hu and Shi's constrained rotated Q_1 element [22], etc. All works listed above concern only lowest order nonconforming elements. Higher order constructions are possible but nontrivial, and are now actively worked on by researchers [23, 25, 27–29].

We aim at developing lowest order Crouzeix-Raviart type nonconforming finite elements on general polygonal meshes. Recall that on polygonal meshes, one can

Received by the editor April 19, 2017, and, in revised form, September 15, 2017, and November 1, 2017.

2010 *Mathematics Subject Classification.* Primary 65N30.

The author was supported by the Natural Science Foundation of China under grant numbers 11671210 and 91630201.

©2018 American Mathematical Society

Licensed to AMS.
License or copyright restrictions may apply to redistribution; see https://www.ams.org/journal-terms-of-use

use generalized barycentric coordinates (GBCs) [16, 18, 41, 43] to construct H^1-conforming finite elements, for example, the Wachspress element [40] and the mean value element [15], etc. It is natural to ask: can we use GBCs to construct a Crouzeix-Raviart type nonconforming element on polygonal meshes? The answer is yes, although nontrivial, and a construction is presented in this paper.

Our construction is of Crouzeix-Raviart type, since each function in the finite element space satisfies: (1) in each polygon, its value on the boundary of the polygon is piecewise-linear; (2) it is continuous across the midpoint of edges. We use GBCs as the building block, i.e., the local finite element space in each polygon is spanned by GBCs. The difficult part is to choose unisolvent local degrees of freedom for polygons with any number of vertices. Inspired by Park and Sheen's simple but profound observation on quadrilaterals [35] that values of a linear function at midpoints of four edges of a quadrilateral are linearly dependent, we reveal a more fundamental rule about the linear dependency of function values at midpoints of edges of a polygon. In short: for functions that are piecewise-linear on the boundary of the polygon, the midpoint values are linearly dependent on polygons with even number of vertices (called "even polygons" for simplicity), and are linearly independent on odd polygons. This not only explains why the local construction of Crouzeix-Raviart type elements must be different on triangles and quadrilaterals, but also leads to a systematic construction of nonconforming elements on general odd and even polygons.

Because of the difference between odd and even polygons, the topological structure of regions consisting of even polygons determines the structure of the global finite element space. Such a fact has already been noticed in [1] and analyzed for triangular-quadrilateral hybrid meshes with simpler structures. But for general polygonal meshes, the mesh structure can be complicated and thus sophisticated mathematical tools become necessary in the analysis. Another major contribution of this paper is to provide such a tool: we found the relation between the structure of even polygon clusters and a special cochain complex. Using its cohomology (a concept often used in algebraic topology) allows one to analyze every detail of the nonconforming finite element space to be constructed.

One may wonder how our construction of a nonconforming element compares with existing ones on triangular or rectangular/quadrilateral meshes. This will be explained with details in Section 2. Here we just give readers a brief idea about it. On triangular meshes, our element coincides with the lowest-order Crouzeix-Raviart element, as expected. On rectangular/quadrilateral meshes, since there exist a variety of generalized barycentric coordinates on a polygon with more than three vertices and our construction is based on GBCs, we actually provide a variety of nonconforming elements depending on which GBC one chooses to use. However, none of these varieties coincides with existing nonconforming elements on rectangular meshes. Indeed, nonconforming elements defined in [7, 14, 21, 30, 36] do not have piecewise-linear local value on the boundary of a rectangle, while our element does. For Park and Sheen's P_1 nonconforming element [35], our element can be viewed as this element plus local bubbles, as will be explained in Section 2. Hu and Shi's constrained rotated Q_1 element [22] is identical to Park and Sheen's P_1 nonconforming element on rectangles, but is different on general quadrilaterals. Thus our element is again different from Hu and Shi's element in general.

Licensed to AMS.
License or copyright restrictions may apply to redistribution; see https://www.ams.org/journal-terms-of-use

We mention that there have been other works on extending the nonconforming element to polygonal/polyhedral meshes. One was given in [2] by using the virtual element method (VEM) [3]. In the lowest order conforming VEM introduced in [3] and references therein, discrete functions have piecewise-linear values on the boundary of mesh polygons/polyhedra. However, the nonconforming VEM in [2] no longer follows this rule since it uses moments to define the degrees of freedom. Consequently, the discrete functions may not be piecewise-linear on the boundary of mesh polygons/polyhedra. Our work is different from [2] in that: (1) our basis functions are explicitly given; (2) our basis functions are piecewise-linear on the boundary of polygons. Indeed, we claim to provide an intuitive and explicit extension of the lowest-order Crouzeix-Raviart element to polygonal meshes. Another work was given in [13], where the authors constructed a generalized Crouzeix-Raviart element by using a fictitious pyramidal subdivison of the original polytopal mesh. In 2014, Di Pietro, Ern, and Lemaire proposed a discretization [12], using polynomial basis functions both inside the polygons/polyhedra and on the edges/faces, for diffusion problems. The method is based on a local (element-wise) discrete gradient reconstruction, and uses a least-squares penalty term to weakly enforce the matching between element- and face-degrees of freedom. The methods in [2, 12, 13] do not require specific mesh structure and have been generalized to high order as well as 3-dimensions, which are the advantages that so far our method has not achieved.

The rest of the paper is organized as follows. Section 2 focuses on the construction of the nonconforming finite element space, which is further divided into five subsections: local basis functions are defined in Subsection 2.1; notation system for the polygonal mesh structure is introduced in Subsection 2.2; the cochain complex and cohomology are presented in Subsection 2.3 (without essential boundary condition) and Subsection 2.4 (with essential boundary condition); and definition and analysis of the global finite element spaces are given in Subsection 2.5. In Section 3, error analysis is presented. Finally, implementation details and numerical results are given in Section 4.

Despite the seemingly complicated theoretical analysis, the implementation of our nonconforming finite element method is quite straightforward. Readers who are only interested in the construction and implementation may skip some "theoretical" sections (2.3–2.4 and Appendices A–B), which shall not affect the understanding of the practical algorithm.

2. The nonconforming finite element space

We first design local basis functions of the nonconforming element on individual polygons, and then glue them together to get global basis functions that span the finite element space. Strictly speaking, the "basis functions" to be constructed may not truly form a basis as they may be linearly dependent. But following the convention, we still call them "basis functions" instead of "spanning set". It will be shown later that, leaving the basis functions linearly dependent does not in general cause much of a problem in the practical implementation. If it does, an easy solution is provided, which drops just enough basis functions until the rest become linearly independent.

2.1. **Local basis functions.** Consider a polygon T with vertices $\mathbf{v}_i$, $i = 1, \ldots, n$, ordered counterclockwisely. Here T can be either convex or nonconvex. Denote by f_i the edge(face) of T connecting vertices $\mathbf{v}_i$ and $\mathbf{v}_{i+1}$, and by $\mathbf{m}_i$ the midpoint

Licensed to AMS.
License or copyright restrictions may apply to redistribution; see https://www.ams.org/journal-terms-of-use

of f_i. Here we use "f" instead of "e" to denote edges(faces) in order to reserve the notation "e" for "even". For convenience, an index i is considered identical to $(i \bmod n)$, which allows one to extend the indices beyond the range of $\{1, \ldots, n\}$. For example, one has $\mathbf{v}_{n+1} = \mathbf{v}_1$ and $\mathbf{m}_0 = \mathbf{m}_n$.

Let $\{\lambda_i\}$, $i = 1, \ldots, n$, be a set of generalized barycentric coordinates (GBCs) [16, 18] on T, i.e., a set of continuous functions satisfying the following:

(1) (Nonnegativity) All λ_i, for $1 \le i \le n$, have nonnegative value on T.
(2) (Linear precision) For any linear function $L(\mathbf{x})$ defined on T, one has

$$L(\mathbf{x}) = \sum_{i=1}^{n} L(\mathbf{v}_i)\lambda_i(\mathbf{x}) \qquad \text{for all } \mathbf{x} \in T.$$

The GBC is a natural extension of the traditional barycentric coordinate on triangles, and is important in designing polygonal finite elements. Several different GBCs have been developed on polygons. As an example, we present a formula for the Wachspress coordinates [32, 40]:

$$\lambda_i(\mathbf{x}) = \frac{w_i(\mathbf{x})}{\sum_{j=1}^{n} w_j(\mathbf{x})} \qquad \text{for } i = 1, \ldots, n,$$

with

$$w_i(\mathbf{x}) = A(\mathbf{v}_{i-1}\mathbf{v}_i\mathbf{v}_{i+1}) \prod_{j \neq i, i-1} A(\mathbf{x}\mathbf{v}_j\mathbf{v}_{j+1}),$$

where $A(\mathbf{xyz})$ denotes the signed area of the triangle with vertices $\mathbf{x}$, $\mathbf{y}$, and $\mathbf{z}$. The Wachspress coordinates are rational functions and are well-defined only on convex polygons. Some other GBCs, like the mean value coordinates [15], work for both convex and nonconvex polygons.

The following important properties of the GBC are well known (see [19] and references therein):

- (Lagrange property) For $1 \le i, j \le n$, one has $\lambda_i(\mathbf{v}_j) = \delta_{ij}$, where δ_{ij} is the Kronecker delta.
- (Trace property) Each λ_i is piecewise-linear on ∂T.

Define the local function space

$$Q_T = span\{\lambda_i,\ i = 1, \ldots, n\}.$$

The space Q_T has been used to construct H^1-conforming finite element methods [19, 38, 39], in which the degrees of freedom (dofs) are nodal values at $\mathbf{v}_i$ and hence H^1-conformity (i.e., C^0-continuity) is guaranteed. Clearly, the linear precision of the GBC immediately implies that $P_1 \triangleq span\{1, x, y\} \subseteq Q_T$.

When considering the nonconforming finite element, we tend to still use Q_T as the local function space. This is because: (1) Q_T is a space with many important properties, especially the trace property and the fact that $P_1 \subseteq Q_T$; (2) the dimension of Q_T is equal to the number of vertices, which provides necessary controllability when gluing local functions together; (3) implementation of GBC has been well studied and thus the local stiffness matrix can be easily computed; (4) when T happens to be a triangle, Q_T coincides with the well-known Crouzeix-Raviart nonconforming finite element space on triangles.

After defining the polygon T and the function space Q_T, the next step is to specify a set of unisolvent degrees of freedom (dofs) for the nonconforming element. One may first think about using nodal values at $\mathbf{m}_i$ as dofs, since they naturally

Licensed to AMS.
License or copyright restrictions may apply to redistribution; see https://www.ams.org/journal-terms-of-use

coincide with the triangular Crouzeix-Raviart dofs. Unfortunately, this simple idea does not work on polygons with even number of vertices, which we call "even polygons" for simplicity ("odd polygons" are named similarly). On even polygons, the function

$$\mu_0 = \lambda_1 - \lambda_2 + \lambda_3 - \lambda_4 + \cdots - \lambda_n \in Q_T \tag{2.1}$$

vanishes at all $\mathbf{m}_i$. In other words, *nodal values at midpoints of edges do not form a unisolvent set of dofs on even polygons.* Such a fact has already been observed by researchers working on quadrilateral nonconforming elements [22, 35]. Here we shall study it from a new perspective by classifying polygons into even and odd. The essential difference between even and odd polygons will be revealed and used to construct different local dofs. Our goal is to eventually build a unified nonconforming method that works on arbitrary polygonal meshes containing odd polygons, even polygons, or both.

For a function $\phi \in Q_T$, we introduce two vector representations of ϕ as

$$\overline{\phi}_v = [\phi(\mathbf{v}_1), \phi(\mathbf{v}_2), \ldots, \phi(\mathbf{v}_n)]^t, \qquad \overline{\phi}_f = [\phi(\mathbf{m}_1), \phi(\mathbf{m}_2), \ldots, \phi(\mathbf{m}_n)]^t.$$

Define two associated linear maps l_v, $l_f : Q_T \to \mathbb{R}^n$ by

$$l_v(\phi) = \overline{\phi}_v, \qquad l_f(\phi) = \overline{\phi}_f.$$

When T is an even polygon, denote

$$\overline{a}_T = [1, -1, 1, -1, \ldots, 1, -1]^t \in \mathbb{R}^n. \tag{2.2}$$

Lemma 2.1. *The map l_v is a bijection and*

when n is odd: *the map l_f is a bijection,*

when n is even: $Ker(l_f) = span\{\mu_0\}$, $Im(l_f) = \mathbb{R}^n / span\{\overline{a}_T\}$.

Proof. By the definition of λ_i, it is clear that l_v is a bijection. Then the relation $\phi(\mathbf{m}_i) = \frac{1}{2}(\phi(\mathbf{v}_i) + \phi(\mathbf{v}_{i+1}))$ on each edge of T leads to a linear transformation

$$\overline{\phi}_f = \frac{1}{2}\begin{bmatrix} 1 & 1 & 0 & 0 & \cdots & 0 \\ 0 & 1 & 1 & 0 & \cdots & 0 \\ 0 & 0 & 1 & 1 & \cdots & 0 \\ & & & \ddots & \ddots & \\ 0 & 0 & 0 & 0 & \ddots & 1 \\ 1 & 0 & 0 & 0 & \cdots & 1 \end{bmatrix} \overline{\phi}_v = l_f \circ l_v^{-1}(\overline{\phi}_v).$$

Denote the matrix representation of $l_f \circ l_v^{-1}$ by L. Using Gaussian elimination, it is clear that

$$Ker(L) = Ker(L^t) = \begin{cases} \emptyset & \text{when } n \text{ is odd,} \\ span\{\overline{a}_T\} & \text{when } n \text{ is even.} \end{cases}$$

Note that $\overline{(\mu_0)}_v = \overline{a}_T$ on even polygons. This completes the proof of the lemma. □

Remark 2.2. On an even polygon T, Lemma 2.1 implies that a function $\phi \in Q_T$ must satisfy

$$\phi(\mathbf{m}_1) - \phi(\mathbf{m}_2) + \phi(\mathbf{m}_3) - \phi(\mathbf{m}_4) + \cdots - \phi(\mathbf{m}_n) = \overline{a}_T \cdot \overline{\phi}_f = 0. \tag{2.3}$$

Licensed to AMS.
License or copyright restrictions may apply to redistribution; see https://www.ams.org/journal-terms-of-use

Moreover, given a vector $\overline{c} \in \mathbb{R}^n$ satisfying $\overline{a}_T \cdot \overline{c} = 0$, then there must exist a function $\phi \in Q_T$, unique up to a constant times μ_0, such that $\phi(\mathbf{m}_i) = \overline{c}_i$ for $i = 1, \ldots, n$.

Now we are able to define local basis functions:

(1) On odd polygons, use nodal values at $\mathbf{m}_i$ as dofs. This leads to a nodal basis $\{\mu_i\}_{i=1}^n$ in Q_T, each of which is uniquely determined by

$$\mu_i(\mathbf{m}_j) = \delta_{ij} \quad \text{for } j = 1, \ldots, n.$$

By elementary linear algebra, one gets

$$\begin{bmatrix} \mu_1 \\ \mu_2 \\ \mu_3 \\ \vdots \\ \mu_{n-1} \\ \mu_n \end{bmatrix} = \begin{bmatrix} 1 & 1 & -1 & 1 & \cdots & -1 \\ -1 & 1 & 1 & -1 & \cdots & 1 \\ 1 & -1 & 1 & 1 & \cdots & -1 \\ & & & \ddots & \ddots & \\ -1 & 1 & -1 & 1 & \ddots & 1 \\ 1 & -1 & 1 & -1 & \cdots & 1 \end{bmatrix} \begin{bmatrix} \lambda_1 \\ \lambda_2 \\ \lambda_3 \\ \vdots \\ \lambda_{n-1} \\ \lambda_n \end{bmatrix}. \tag{2.4}$$

The coefficient matrix, denoted by B, satisfies $B_{i,i} = B_{i,i+1} = 1$ while all other entries are alternating 1's and -1's. By Gaussian elimination, this matrix is nonsingular and hence one has $span\{\mu_i, i = 1, \ldots, n\} = span\{\lambda_i, i = 1, \ldots, n\} = Q_T$.

When T is a triangle, the above construction gives exactly the lowest order Crouzeix-Raviart element.

(2) On even polygons, the local basis functions are defined differently. Since l_v is a bijection, we first introduce a decomposition of space $Q_T = Q_{0,T} \oplus \hat{Q}_T$ as follows:

$$Q_{0,T} \triangleq span\{\mu_0\},$$

$$\begin{aligned} \hat{Q}_T &\triangleq \{\phi \in Q_T \,|\, l_v(\phi) \perp l_v(\mu_0)\} \\ &= \{\phi \in Q_T \,|\, \phi(\mathbf{v}_1) - \phi(\mathbf{v}_2) + \phi(\mathbf{v}_3) - \phi(\mathbf{v}_4) + \cdots - \phi(\mathbf{v}_n) = 0\}. \end{aligned} \tag{2.5}$$

That is, the images of $Q_{0,T}$ and $\hat{Q}_T$ under the map l_v are orthogonal. Then we pick a spanning set for $\hat{Q}_T$ as follows:

$$\mu_i = 2\Big(\lambda_i + \frac{(-1)^i}{n}\mu_0\Big) \qquad \text{for } i = 1, \ldots, n,$$

i.e.,

$$\begin{bmatrix} \mu_1 \\ \mu_2 \\ \mu_3 \\ \vdots \\ \mu_{n-1} \\ \mu_n \end{bmatrix} = \frac{2}{n} \begin{bmatrix} n-1 & 1 & -1 & 1 & \cdots & 1 \\ 1 & n-1 & 1 & -1 & \cdots & -1 \\ -1 & 1 & n-1 & 1 & \cdots & 1 \\ & & & \ddots & \ddots & \\ & & & & \ddots & 1 \\ 1 & -1 & 1 & -1 & \cdots & n-1 \end{bmatrix} \begin{bmatrix} \lambda_1 \\ \lambda_2 \\ \lambda_3 \\ \vdots \\ \lambda_{n-1} \\ \lambda_n \end{bmatrix}. \tag{2.6}$$

The coefficient matrix, denoted by D, satisfies $D_{i,i} = 2\frac{n-1}{n}$, $D_{i,i+1} = D_{i+1,i} = \frac{2}{n}$ while all other entries are alternating $\frac{2}{n}$'s and $-\frac{2}{n}$'s. One has $\mu_i \in \hat{Q}_T$ since each row of the matrix D is orthogonal to $l_v(\mu_0) = \overline{a}_T$.

Licensed to AMS.
License or copyright restrictions may apply to redistribution; see https://www.ams.org/journal-terms-of-use

Lemma 2.3. *On even polygons,* $\{\mu_i\}_{i=1}^n$ *is linearly dependent and spans* $\hat{Q}_T$.

Proof. $\{\mu_i\}_{i=1}^n$ is linearly dependent since

$$\mu_1 - \mu_2 + \mu_3 - \mu_4 + \cdots - \mu_n = 0.$$

Note that $rank(D) \geq n-1$ since diagonally dominant matrices have at most a rank 1 deficiency. Indeed, $rank(D)$ is $n-1$ since it is obvious that $\overline{a}_T \in Ker(D)$. Because D is symmetric, one has $Im(D) = \mathbb{R}/span\{\overline{a}_T\} = l_v(\hat{Q}_T)$. This completes the proof of the lemma. □

In conclusion, $\{\mu_0, \mu_1, \ldots, \mu_n\}$ spans the space Q_T and hence is set to be the "local basis functions" on an even polygon T. We also point out that μ_i, for $i = 1, \ldots, n$, satisfies

$$\mu_i(\mathbf{m}_j) = \begin{cases} 1 & \text{for } j = i-1,\ i, \\ 0 & \text{otherwise,} \end{cases}$$

while μ_0 vanishes at all $\mathbf{m}_j$ and can be viewed as a "bubble function".

Remark 2.4. On even polygons, the idea of picking μ_i such that its values on $\mathbf{m}_{i-1}$ and $\mathbf{m}_i$ are 1 actually makes μ_i associated with vertex $\mathbf{v}_i$. We learned this from Park and Sheen's work [35] on constructing a P_1 nonconforming element for quadrilateral meshes. Park and Sheen's element was further studied by Altmann and Carstensen [1] for triangular-quadrilateral hybrid meshes. When T is a rectangle, the space $\hat{Q}_T$ is exactly P_1 and thus our construction is just Park and Sheen's P_1 element plus a bubble function μ_0. On general quadrilaterals, $\hat{Q}_T$ may be different from P_1. Recall that Hu and Shi's constrained rotated Q_1 element [22] is identical to Park and Sheen's P_1 nonconforming element on rectangular meshes. Thus our element is also different from Hu and Shi's element in general.

One may wonder whether it is possible to drop μ_0 and simply use $\hat{Q}_T$ in the construction. On rectangles this is fine and will lead to Park and Sheen's [35]. But on general even polygons, we may not have $P_1 \subseteq \hat{Q}_T$, which is essential to the theoretical error analysis. However, numerical results suggest that such "reduced" construction works quite well, as will be shown in Subsection 4.4.

Remark 2.5. On rectangular meshes, our nonconforming element, which has piecewise-linear local values on the boundary of rectangles, is different from several existing rectangular nonconforming finite elements proposed in [7, 14, 21, 30, 36], which add nonbilinear terms to the finite element space and hence no longer have piecewise-linear boundary data.

2.2. **Polygonal mesh structure.** Since there is a fundamental difference between odd and even polygons, we therefore first introduce concepts regarding the even-odd mesh structure. A similar but less general structure has been studied in [1] for triangular-quadrilateral hybrid meshes. Once all concepts are clarified, an easy-to-use notation system will be presented.

Let $\mathcal{T}$ be a polygonal mesh on a connected polygonal domain Ω. In order to achieve expected approximation properties, $\mathcal{T}$ needs to satisfy certain mesh regularity conditions. We postpone such discussion until the next section, as we shall

Licensed to AMS.
License or copyright restrictions may apply to redistribution; see https://www.ams.org/journal-terms-of-use

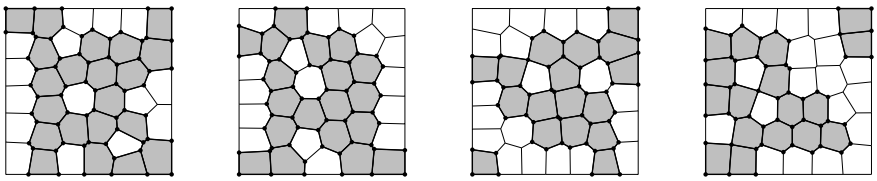

(A) (B) (C) (D)

FIGURE 1. Even polygons are marked with gray, even edges are drawn in thick lines, and even vertices are marked by dots. By splitting singular vertices into phantoms, the large E-region in (C) contains no hole and the large one in (D) contains only one hole.

focus on the even-odd structure here. To incorporate the Dirichlet boundary condition defined on part of the boundary $\Gamma_D \subseteq \partial\Omega$, if there is any, we say a vertex or an edge is "interior" as long as it does not lie on $\overline{\Gamma}_D$, the closure of Γ_D.

We classify polygons, edges, and vertices in mesh $\mathcal{T}$ as follows:

- Polygons are divided into even and odd polygons according to their number of vertices.
- Edges are divided into even and odd edges. An edge is even if it lies on the boundary of an even polygon. Otherwise, it is odd.
- Vertices are divided into even and odd vertices. A vertex is even if it is a vertex of an even polygon. Otherwise, it is odd.

By coloring all even polygons gray, as in Figure 1, one immediately sees that even polygons/edges/vertices are forming a submesh of $\mathcal{T}$. In Figure 1(C)(D), we notice a type of "bad" vertex which makes the boundary of the gray region non-Lipschitz. Such a "bad" vertex needs to be split into multiple vertices in both the analysis and the algorithm. To this end, we first borrow the following concept of "edge-connected" from [1].

Definition 2.6. Two even polygons T_1 and T_2 are edge-connected, denoted by $T_1 \sim T_2$, if they share a common edge, or if there is a finite chain of even polygons $T_1, T_{1.1}, T_{1.2}, \ldots, T_{1.k}, T_2$ such that every two consecutive polygons are edge-connected. The relation $\sim$ is an equivalence relation and thus defines equivalence classes. Each equivalence class is called an E-region R.

Note that an E-region R can also be viewed as a connected closed subdomain with its own boundary ∂R. All vertices and edges in an E-region are even.

We say an even vertex is singular (the "bad" vertex) if the boundary of an E-region is non-Lipschitz at the vertex, i.e., multiple pieces of boundary touch each other. Each singular even vertex shall be split into and counted as multiple phantoms, one for each touching E-region (see Figure 2(B)–(F)). When a singular even vertex lies on $\overline{\Gamma}_D$, its phantom associated with E-regions connected to Γ_D is considered a boundary phantom, as shown in Figure 2(D)(F). Otherwise, it is an interior phantom, as in Figure 2(E)(F). In the rest of this paper, when we talk about even vertices, phantoms are counted instead of the original singular vertex.

E-regions may contain holes formed by odd polygons and/or holes of Ω, if Ω is not simply connected. But thanks to the introduction of phantom vertices, each E-region can now be viewed as a connected domain with Lipschitz boundary. One

Licensed to AMS.
License or copyright restrictions may apply to redistribution; see https://www.ams.org/journal-terms-of-use

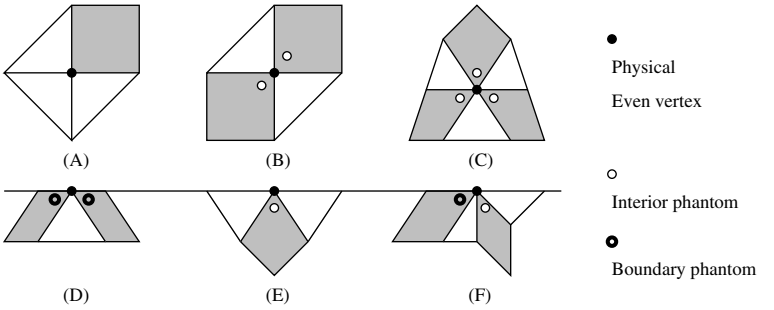

FIGURE 2. When E-regions, marked with gray, meet at an even vertex, this even vertex is singular and shall be split into multiple phantoms, as shown in subfigures (B)–(F). Subfigure (A) shows a normal even vertex. The thick line in (D)–(F) is Γ_D.

shall note that a singular even vertex, split into multiple phantoms, can no longer form new holes in an E-region, as shown in Figure 1(C)(D). The structure of E-regions in large polygonal meshes can be complicated, as they may contain holes which in turn contain E-regions inside (see Figure 3).

For an E-region R, define an E-boundary component B to be a maximum connected subset of ∂R. Each E-boundary component is a closed curve formed by even edges in $\mathcal{T}$. We say an E-boundary component is odd/even if it contains an odd/even number of edges. Moreover, we say an E-region is even if it has only even E-boundary components. An E-region is odd if it has at least one odd E-boundary component. By counting the number of edges and noticing that E-regions contain only even polygons, one has:

Lemma 2.7. *A simply connected E-region has only one even E-boundary component and hence is an even E-region. In a general E-region, the total number of odd E-boundary components must be even.*

We say an E-boundary component B is interior if $B \cap \overline{\Gamma}_D$ contains at most singular even vertices; B is on the boundary if $B \subseteq \overline{\Gamma}_D$; and B is of mixed type if only part of B lies on $\overline{\Gamma}_D$. We say an E-region R is interior if all its E-boundary components are interior, and we say R is "on the boundary" if $\partial R \subseteq \overline{\Gamma}_D$. Since Ω is connected, there exists at most one E-region R on the boundary and in this case R fills the entire domain Ω with $\partial\Omega = \Gamma_D$.

Next, we introduce a straightforward notation system to denote the sets of different entities defined so far:

$$(NAME)^*_{*,*},$$

where

(1) $NAME$ means the name of the entity. We use V, F, T, R, and B to denote "vertex", "face(edge)", "polygon", "E-region", and "E-boundary component", respectively. Calligraphic font means the set of a type of entities, while an extra # in the front means cardinality of the corresponding set.
(2) The superscript is optional. It can be i (interior), b (on the boundary), or m (of mixed type). If there is no superscript, then all cases are included.

Licensed to AMS.
License or copyright restrictions may apply to redistribution; see https://www.ams.org/journal-terms-of-use

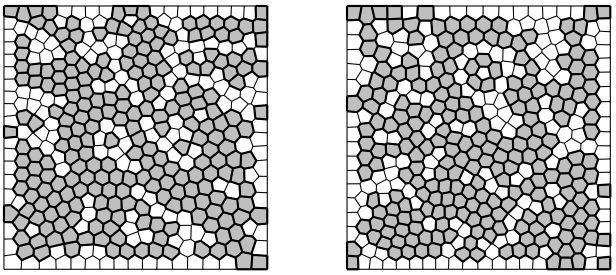

(A) (B)

FIGURE 3. E-regions may contain a hole with another E-region inside the hole.

Such a rule also applies to the optional first and second subscripts. The designation i works for vertices, edges, E-regions, and E-boundary components, b works for E-regions and E-boundary components, and m is only defined for E-boundary components.

(3) The optional first subscript can be o (odd) or e (even).
(4) The optional second subscript is an E-region: it means only entities in this E-region are considered.

We list a few examples to illustrate this notation system:

$\mathcal{V}$ — set of all vertices;

$\#F_o^i$ — number of all interior odd edges (cardinality of $\mathcal{F}_o^i$);

$\mathcal{B}_R$ — set of all E-boundary components in E-region R;

$\mathcal{B}_o^m$ — set of all odd E-boundary components of mixed type;

$\#R_e^i$ — number of all interior even E-regions;

$\mathcal{R}^b$ — set of boundary E-region: it is either empty or contains only one E-region filling the entire Ω; in this case $\Gamma_D = \partial\Omega$.

Sometimes, the same set can be expressed in more than one way. For example, $\mathcal{V}_R = \mathcal{V}_{e,R}$ for all $R \in \mathcal{R}$, because all vertices in an E-region must be even.

The notation introduced above allows one to easily describe properties of E-regions. For example, note that each E-region R can be viewed topologically as an orientable compact surface with boundary, and thus can be studied by topological tools such as the Euler characteristic [26]:

$$\chi(R) = 2 - \#B_R.$$

Then, by Lemma 2.7, one has $\chi(R) \leq 1$ for even E-regions and $\chi(R) \leq 0$ for odd E-regions. It is also well known that (or one can easily prove it by induction)

$$\#V_R - \#F_R + \#T_R = \chi(R). \tag{2.7}$$

Finally, we mention that, fortunately, most of the mesh structures defined in this subsection are for theoretical analysis. Only two of them are required in the practical implementation: (1) even/odd mark for polygons, edges, and vertices;

Licensed to AMS.
License or copyright restrictions may apply to redistribution; see https://www.ams.org/journal-terms-of-use

(2) phantoms and their associated E-regions. In Subsection 4.1, we shall discuss efficient implementation of these two data structures.

2.3. **Even submesh, cochain complex, and cohomology.** This subsection and the next one are meant for theoretical analysis. It will be helpful to know basic definitions of cochain complex and cohomology, which can be found in any algebraic topology textbook (for example [34,37]), before moving on, although we have carefully arranged the presentation style so that readers with only general knowledge of linear algebra shall be able to follow. Those who are only interested in the implementation can jump to Subsection 2.5 directly.

Notice that *even polygons, edges, and vertices form a polygonal submesh* on the union of all E-regions. In this subsection, we introduce new tools to study this even submesh. To be more specific, let Ω_e be the union of all E-regions, shown as the gray part in Figures 1–3. Then $\mathcal{T}_e$ is a well-defined polygonal mesh on Ω_e with set of edges $\mathcal{F}_e$ and set of vertices $\mathcal{V}_e$. Again, thanks to the introduction of phantom vertices, Ω_e *can be viewed as having Lipschitz boundary.*

In this subsection, we only consider the situation when $\Gamma_D = \emptyset$, i.e., all mesh entities are interior. The case $\Gamma_D \neq \emptyset$ will be discussed in the next subsection.

It is convenient to call vertices, edges, and polygons p-cells, for $p = 0, 1, 2$, respectively. Denote by $\mathcal{K}$ the collection of all p-cells in $\{\mathcal{T}_e, \mathcal{F}_e, \mathcal{V}_e\}$. Let d_p be the number of p-cells in $\mathcal{K}$, i.e., $d_0 = \#V_e$, $d_1 = \#F_e$, and $d_2 = \#T_e$. For $p = 0, 1, 2$, assign a global index to even p-cells, that is, 0-cells are indexed from 1 to d_0, 1-cells from 1 to d_1, and 2-cells from 1 to d_2. A p-covector is a vector $\bar{c}^p \in \mathbb{R}^{d_p}$ such that its ith entry is considered as associated with the ith p-cell. For 1-cells (edges), this association occurs at the midpoint of the edge. The space of all p-covectors is denoted by $C^p(\mathcal{K}) = \mathbb{R}^{d_p}$.

Define the coboundary operator $\Pi^p : C^p(\mathcal{K}) \to C^{p+1}(\mathcal{K})$, for $p = 0, 1$, as a matrix in $\mathbb{R}^{d_{p+1} \times d_p}$ with entries satisfying

$$[\Pi^0]_{ij} = \begin{cases} 1 & \text{if the } j\text{th even vertex is an end of the } i\text{th even edge,} \\ 0 & \text{otherwise,} \end{cases}$$

$$[\Pi^1]_{ij} = \begin{cases} 1 & \text{if the } j\text{th even edge is an edge, with odd local index,} \\ & \quad \text{of the } i\text{th even polygon,} \\ -1 & \text{if the } j\text{th even edge is an edge, with even local index,} \\ & \quad \text{of the } i\text{th even polygon,} \\ 0 & \text{otherwise.} \end{cases}$$

Here the local index of an edge in a polygon is the index introduced in Subsection 2.1, which is related to the definition of local basis functions of the nonconforming element. Then, it is not hard to see that $\Pi^1\Pi^0 = 0$, i.e., $Im(\Pi^0) \subseteq Ker(\Pi^1)$. Indeed, this can be verified by checking if $\Pi^1\Pi^0$ vanishes or not on a basis of $C^0(\mathcal{K})$, consisting of covectors with value 1 on one vertex and 0 elsewhere. An illustration is given in Figure 4. Therefore,

$$0 \longrightarrow C^0(\mathcal{K}) \xrightarrow{\Pi^0} C^1(\mathcal{K}) \xrightarrow{\Pi^1} C^2(\mathcal{K}) \longrightarrow 0 \tag{2.8}$$

is a cochain complex, although it is not necessarily an exact sequence, which further requires $Im(\Pi^0) = Ker(\Pi^1)$.

Licensed to AMS.
License or copyright restrictions may apply to redistribution; see https://www.ams.org/journal-terms-of-use

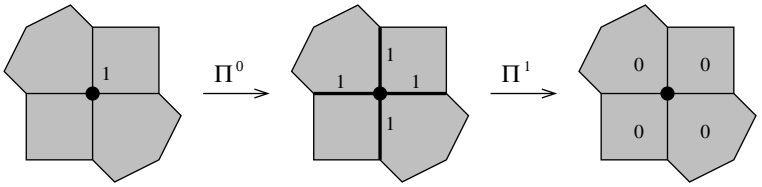

FIGURE 4. An example showing that $\Pi^1\Pi^0$ vanishes on a basis of $C^0(\mathcal{K})$. In the left graph, we draw a covector $\bar{c}^0 \in C^0(\mathcal{K})$ whose value is 1 at the even vertex marked by a black dot, and 0 at all other even vertices. In the center graph, notice that $\Pi^0\bar{c}^0$ has nonzero entries (with value equal to 1) only at those even edges (marked by thick lines) connected to the marked vertex. In the right graph, one can see that $\Pi^1\Pi^0\bar{c}^0$ has value 0 on all even polygons, by using the definition of Π^1.

Following the conventional terminology of algebraic topology, elements of $ker(\Pi^1)$ and $Im(\Pi^0)$ are called cocycles and coboundaries, and elements in $ker(\Pi^1)/Im(\Pi^0)$ form cohomology classes. We shall see in Subsection 2.5 that $ker(\Pi^1)$ and $Im(\Pi^0)$ are closely related to the nonconforming finite element spaces.

Remark 2.8. Chain and cochain complexes on simplicial meshes [34, 37] have been studied in algebraic topology since Poincaré. Traditional definitions of chain and cochain complexes use abelian groups of oriented p-simplices, and can be easily generalized into cellular meshes. They have caught the attention of numerical analysts since they can handle mesh data structures easily [6, 20].

Our cochain complex (2.8) is completely different from the traditional definition as it uses nonoriented p-cells. The complex (2.8) can only be defined for meshes consisting of even polygons. We believe that we are the first to discover this type of cochain complex as well as its application in numerical analysis. The cochain complex (2.8) has an accompanying chain complex, which is irrelevant to this paper and hence omitted.

The coboundary operators are matrices and hence elementary linear algebra is enough for analyzing the cohomology of the cochain complex (2.8). For each E-region R, define an "alternating $C^0(\mathcal{K})$ vector on R" to be a vector in $C^0(\mathcal{K})$ such that: (1) its entries associated with all even vertices in $\mathcal{V}_R$ have the same absolute value, while every two entries associated with two ends of an edge take opposite signs; (2) its entries on even vertices out of R are 0. Denote by $\mathscr{A}_R \subseteq C^0(\mathcal{K})$ the space of all alternating $C^0(\mathcal{K})$ vectors on R. Then one has

Lemma 2.9. *The dimension of $\mathscr{A}_R$ satisfies*

$$dim(\mathscr{A}_R) = \begin{cases} 1 & \text{for even E-region } R, \\ 0 & \text{for odd E-region } R. \end{cases}$$

Lemma 2.9 and other lemmas in the rest of this subsection will be proved in Appendix A.

Licensed to AMS.
License or copyright restrictions may apply to redistribution; see https://www.ams.org/journal-terms-of-use

Lemma 2.10. *The operator* Π^0 *satisfies*

$$Ker(\Pi^0) = \bigoplus_{R\in\mathcal{R}_e} \mathscr{A}_R,$$

and hence its dimension is $nullity(\Pi^0) = \#R_e$. *Consequently, the dimension of* $Im(\Pi^0)$ *is* $rank(\Pi^0) = \#V_e - \#R_e$.

Lemma 2.11. *The dimension of* $Ker(\Pi^1)$ *is*

$$nullity(\Pi^1) = \#F_e - \#T_e.$$

It is clear that $\#V_e \geq \#R_e$ and $\#F_e \geq \#T_e$. Hence $rank(\Pi^0)$ and $nullity(\Pi^1)$ are nonnegative. From Lemma 2.7 and equation (2.7) one gets $rank(\Pi^0) \leq nullity(\Pi^1)$, which agrees well with the fact that $Im(\Pi^0) \subseteq Ker(\Pi^1)$. Moreover, the dimension of the cohomology space $Ker(\Pi^1)/Im(\Pi^0)$ is just $nullity(\Pi^1) - rank(\Pi^0)$. The cohomology is related to the hole structure of E-regions, as expected. To get a basis (or a spanning set) of the cohomology space, we borrow the concept "edge path" from [1]. Let B_1 and B_2 be two different E-boundary components in an E-region R. Pick a chain of edge-connected even polygons in R that connects B_1 with B_2, as shown in darker gray in Figure 5(A). The edges interior to this chain, plus two edges where the chain touches B_1 and B_2, form an "edge path" between two E-boundary components, as shown in thick lines in Figure 5. If the even polygon at the end of the chain touches B_1 or B_2 in more than one edge, then only one of the edges is picked to mark the end of the edge path. Associate $+1$ or -1 to edges in an edge path and 0 to all other edges such that the associated numbers satisfy constraint (2.3) on each polygon. This defines a vector $\bar{p}(B_1, B_2) \in Ker(\Pi^1) \subset C^1(\mathcal{K})$, which will be the building block for $Ker(\Pi^1)/Im(\Pi^0)$. Vector $\bar{p}(B_1, B_2)$ can be shifted (Figure 5(A)) by combining with vectors in $Im(\Pi^0)$, or merged (Figure 5(B)). Thus the choice of particular paths does not matter in the definition of $\bar{p}(B_1, B_2)$, when considered as an equivalence class in the quotient space $Ker(\Pi^1)/Im(\Pi^0)$. In the rest of this paper, with a slight abuse of notation, we also use $\bar{p}(B_1, B_2)$ to represent its equivalence class in the cohomology $Ker(\Pi^1)/Im(\Pi^0)$.

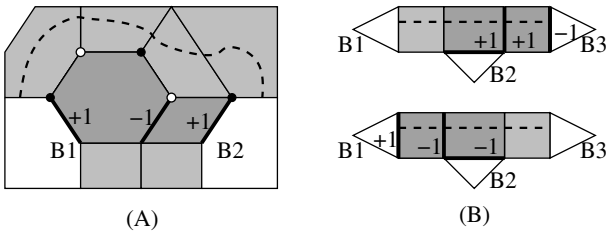

FIGURE 5. Edge paths. The chain of edge-connected even polygons defining the path is shown in darker gray and edges in the path are drawn in thick lines. (A) $\bar{p}(B_1, B_2)$ can be shifted to a new edge path, marked with a dashed curve, by adding vector $\Pi^0(\bar{c}^0) \in Im(\Pi^0)$, where $\bar{c}^0 \in C^0(\mathcal{K})$ takes value $+1/-1$ on circled/solid vertices in the graph and 0 elsewhere. (B) Two edge paths can be merged to a new one marked with a dashed curve, expressed by $\bar{p}(B_1, B_2)+\bar{p}(B_2, B_3) = \bar{p}(B_1, B_3)$ in $Ker(\Pi^1)/Im(\Pi^0)$.

Licensed to AMS.
License or copyright restrictions may apply to redistribution; see https://www.ams.org/journal-terms-of-use

For a given E-region R, fix an anchoring E-boundary component $B \in \mathcal{B}_R$ and define a set with $\#B_R - 1$ vectors:

$$\mathbb{D}_R = \{\bar{p}(B, B') \text{ for } B' \in \mathcal{B}_R \text{ and } B' \neq B\}. \tag{2.9}$$

Then we define the following subspace of $Ker(\Pi^1)/Im(\Pi^0)$:

$$\mathscr{D}_R = span\{\mathbb{D}_R\}.$$

Due to the shifting and combining properties of edge paths, the space $\mathscr{D}_R$ is independent of the choice of the anchoring E-boundary component B or the particular edge path defining vector $\bar{p}(B, B')$. Indeed, one immediately sees that $\mathscr{D}_R$ contains all possible $\bar{p}(B_1, B_2)$ for arbitrary choices of B_1, $B_2 \in \mathcal{B}_R$ and edge paths connecting them.

Lemma 2.12. *The dimension of $\mathscr{D}_R$ satisfies*

$$dim(\mathscr{D}_R) = \begin{cases} \#B_R - 1 & \text{for even E-region } R, \\ \#B_R - 2 & \text{for odd E-region } R. \end{cases}$$

Since each even/odd E-region has at least one/two E-boundary components, one has $dim(\mathscr{D}_R) \geq 0$. Then, we come to the most important result of this subsection.

Lemma 2.13. *The cohomology of cochain complex* (2.8) *satisfies*

$$Ker(\Pi^1)/Im(\Pi^0) = \bigoplus_{R \in \mathcal{R}} \mathscr{D}_R,$$

and $dim(Ker(\Pi^1)/Im(\Pi^0)) = \#R_e - \sum_{R\in\mathcal{R}} \chi(R) \geq 0$, which is equal to

$$nullity(\Pi^1) - rank(\Pi^0) = \#F_e - \#T_e - \#V_e + \#R_e.$$

By Lemma 2.13 and equation (2.7), one has the following corollary.

Corollary 2.14. *$Ker(\Pi^1) = Im(\Pi^0)$ if and only if all odd E-regions have $\#B_R = 2$ and all even E-regions have $\#B_R = 1$, i.e., all odd E-regions have exactly two E-boundary components and all even E-regions have exactly one.*

Finally, we mention a modification of the edge path. Consider an edge path connecting two odd E-boundary components B_1 and B_2. Then $\bar{p}(B_1, B_2)$ can be shifted into an "edge loop" by adding vectors in $Im(\Pi^0)$, as shown in Figure 6(A)(B). The vector associated with the edge loop, still denoted by $\bar{p}(B_1, B_2)$ since they are in the same equivalence class in $Ker(\Pi^1)/Im(\Pi^0)$, has entries equal to either $+\frac{1}{2}$ or $-\frac{1}{2}$ on edges in the loop, and 0 elsewhere. Such a transition to the edge loop does not work for even E-boundary components. But when one of B_1, B_2 is odd and another one is even, we can similarly define a degenerate edge loop, as shown in Figure 6(C). The degenerate edge loop is attached to an edge on the even E-boundary component. The entry of $\bar{p}(B_1, B_2)$ associated with this edge is either $+1$ or -1, while the entries associated with other edges in the loop are still $+\frac{1}{2}$ or $-\frac{1}{2}$.

For any given even E-boundary component, one may similarly define a "fake" edge loop around it (see Figure 6(D)). The vector defined on such a "fake" edge loop, following the same rule as for edge loops, is just a linear combination of vectors in $Im(\Pi^0)$, and hence is identical to $\mathbf{0}$ in $Ker(\Pi^1)/Im(\Pi^0)$.

Two edge loops, including degenerate or "fake" ones, can be merged into a bigger loop, as shown in Figure 6(D)(E).

Licensed to AMS.
License or copyright restrictions may apply to redistribution; see https://www.ams.org/journal-terms-of-use

Remark 2.15. Note that $\#B_{o,R}$ must be an even number. Divide the set $\mathcal{B}_{o,R}$ into E-boundary component pairs, define a nondegenerate edge loop for each pair, and then merge all these edge loops into one. This gives a maximum nondegenerate edge loop that encloses all $B \in \mathcal{B}_{o,R}$, i.e., the other side of this loop, be it the inner or outer side, contains only even E-boundary components. This maximum edge loop then becomes a "fake" loop. In other words, we have found a combination of $\bar{p}(*,*)$ that equals $\mathbf{0}$ in $Ker(\Pi^1)/Im(\Pi^0)$. This explains, from another perspective, why the space $\mathscr{D}_R$ for odd E-region R loses one dimension, as stated in Lemma 2.12.

Replacing the edge path by the edge loop in the definition of $\bar{p}(*,*)$, when applicable, is important in dealing with Dirichlet boundary conditions, as we shall see in the next subsection.

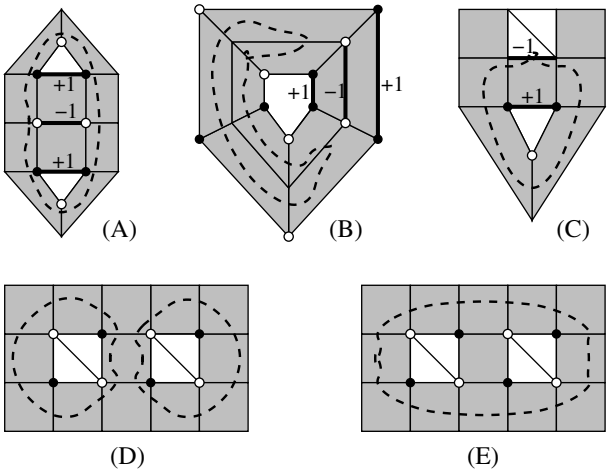

FIGURE 6. Edge loops. (A) An edge path (marked in thick lines) is shifted to an edge loop (marked in a dashed curve) by adding vector $\Pi^0(\bar{c}^0) \in Im(\Pi^0)$, where $\bar{c}^0$ takes value $+\frac{1}{2}/-\frac{1}{2}$ on circled/solid vertices and 0 elsewhere; (B) the shifting can also happen between outer and inner E-boundary components; (C) edge path between even and odd E-boundary components shifted to a degenerate edge loop, attached to an edge on the even E-boundary component; (D) two "fake" edge loops, each enclosing an even E-boundary component; (E) the two edge loops in (D) merged into a bigger loop.

2.4. **Dealing with the Dirichlet boundary condition.** We introduce a subcomplex of the cochain complex (2.8) that incorporates the Dirichlet boundary condition. Let $C_0^p(\mathcal{K}) \in C^p(\mathcal{K})$ be the subspace derived by setting entries associated with boundary p-cells, i.e., p-cells on $\overline{\Gamma}_D$, to be 0. Note this is only effective for $p = 0, 1$, i.e., vertices and edges on $\overline{\Gamma}_D$. Then the restriction of the cochain complex (2.8) on $C_0^p(\mathcal{K})$ is still a cochain complex, i.e.,

$$0 \longrightarrow C_0^0(\mathcal{K}) \xrightarrow{\Pi^0} C_0^1(\mathcal{K}) \xrightarrow{\Pi^1} C_0^2(\mathcal{K}) \longrightarrow 0. \tag{2.10}$$

Licensed to AMS.
License or copyright restrictions may apply to redistribution; see https://www.ams.org/journal-terms-of-use

However, such a simple restriction may have missed something since

$$\tilde{C}_0^0(\mathcal{K}) \triangleq \{\bar{c}^0 \in C^0(\mathcal{K}) \text{ such that } \Pi^0(\bar{c}^0) \in C_0^1(\mathcal{K})\}$$

might be bigger than $C_0^0(\mathcal{K})$, as we shall explain below.

Note that vectors in $\tilde{C}_0^0(\mathcal{K})$ but not in $C_0^0(\mathcal{K})$, if there are any, must have alternating patterns over vertices on $B \cap \overline{\Gamma}_D$, for $B \in \mathcal{B}$, in order to ensure that their images under Π^0 lie in $C_0^1(\mathcal{K})$. This allows one to explicitly spell out the structure of $\tilde{C}_0^0(\mathcal{K}) \backslash C_0^0(\mathcal{K})$. For each maximum connected segment $\gamma \subseteq B \cap \overline{\Gamma}_D$ when $B \in \mathcal{B}_e^b \cup \mathcal{B}^m$, define a vector $\bar{c}_\gamma^0 \in \tilde{C}_0^0(\mathcal{K})$ such that its entries associated with vertices on $\overline{\gamma}$ takes $+1$ and -1 alternatively, and all other entries are 0. For $B \in \mathcal{B}_o^b$, the alternating pattern cannot exist since $\gamma = B \cap \overline{\Gamma}_D$ is a closed curve containing an odd number of edges(vertices), and we formally set $\bar{c}_\gamma^0 = \mathbf{0}$ for convenience. For $B \in \mathcal{B}^i$, there is no γ since $B \cap \overline{\Gamma}_D$ is empty. Thus we define, for each $B \in \mathcal{B}$,

$$\mathbb{G}_B = \{\bar{c}_\gamma^0 \text{ for each maximum connected segment } \gamma \subseteq B \cap \overline{\Gamma}_D\} \tag{2.11}$$

and

$$\mathscr{G}_B = span\{\mathbb{G}_B\}.$$

Denote by $\eta(B)$ the number of disjoint segments in $B \cap \overline{\Gamma}_D$ for $B \in \mathcal{B}_e^b \cup \mathcal{B}^m$, and set $\eta(B) = 0$ for all other $B \in \mathcal{B}$. Then clearly the set $\mathbb{G}_B$ is linearly independent and $dim(\mathscr{G}_B) = \eta(B)$. Define $\mathscr{G} = \bigoplus_{B \in \mathcal{B}} \mathscr{G}_B$, in which the direct sum is obvious. Then one has

$$\tilde{C}_0^0(\mathcal{K}) = C_0^0(\mathcal{K}) \oplus \mathscr{G}, \tag{2.12}$$

where the direct sum is again obvious. Let $\Pi_0^0 = \Pi^0|_{\tilde{C}_0^0(\mathcal{K})}$ and $\Pi_0^1 = \Pi^1|_{C_0^1(\mathcal{K})}$. Then

$$0 \longrightarrow \tilde{C}_0^0(\mathcal{K}) \xrightarrow{\Pi_0^0} C_0^1(\mathcal{K}) \xrightarrow{\Pi_0^1} C_0^2(\mathcal{K}) \longrightarrow 0 \tag{2.13}$$

is a more complete cochain complex comparing to (2.10).

The proofs of the lemmas presented in this subsection will be given in Appendix B.

Lemma 2.16. *One has*

$$Ker(\Pi_0^0) = \bigoplus_{R \in \mathcal{R}_e} \mathscr{A}_R,$$

with $nullity(\Pi_0^0) = \#R_e$ *and hence* $rank(\Pi_0^0) = \#V_e^i + \sum_{B \in \mathcal{B}} \eta(B) - \#R_e$.

By elementary linear algebra, one immediately gets the following corollary.

Corollary 2.17. *The restriction of operator* Π_0^0 *on the subspace* $C_0^0(\mathcal{K})$ *has kernel*

$$Ker(\Pi_0^0) \cap C_0^0(\mathcal{K}) = \bigoplus_{R \in \mathcal{R}_e} \mathscr{A}_R \cap C_0^0(\mathcal{K}) = \bigoplus_{R \in \mathcal{R}_e^i} \mathscr{A}_R.$$

Thus by the rank-nullity relation, the space $\Pi_0^0(C_0^0(\mathcal{K}))$ *has dimension* $\#V_e^i - \#R_e^i$.

Remark 2.18. It is clear that $\tilde{C}_0^0(\mathcal{K}) = C_0^0(\mathcal{K})$ only when $\mathscr{G}$ is trivial, that is, all E-boundary components have $\eta(B) = 0$, i.e., lie in $\mathcal{B}_o^b \cup \mathcal{B}^i$. However, the images of $\tilde{C}_0^0(\mathcal{K})$ and $C_0^0(\mathcal{K})$ under Π_0^0 might be equal even when $\mathscr{G}$ is nontrivial. From Lemma 2.16 and Corollary 2.17, it is not hard to see that

$$\Pi_0^0(C_0^0(\mathcal{K})) = \Pi_0^0(\tilde{C}_0^0(\mathcal{K}))$$

Licensed to AMS.
License or copyright restrictions may apply to redistribution; see https://www.ams.org/journal-terms-of-use

if and only if: (1) each even E-region R has $\sum_{B\in\mathcal{B}_R}\eta(B)\le 1$; (2) each odd E-region R has $\sum_{B\in\mathcal{B}_R}\eta(B)=0$. In this case we have $rank(\Pi_0^0)=\#V_e^i-\#R_e^i$.

Lemma 2.19. *The dimension of* $Ker(\Pi_0^1)$ *is*

$$nullity(\Pi_0^1)=\#F_e^i-\#T_e+\#R_e^b.$$

Although requiring a little deduction, it is not hard to see that both $rank(\Pi_0^0)$ and $nullity(\Pi_0^1)$ are nonnegative. Indeed we also have $rank(\Pi_0^0)\le nullity(\Pi_0^1)$, which will become clear by the end of this subsection. To study the cohomology $Ker(\Pi_0^1)/Im(\Pi_0^0)$, again we need to use the space $\mathscr{D}_R$ spanned by $\mathbb{D}_R$, as defined in (2.9). However, now the edge paths defining vectors in $\mathbb{D}_R$ must avoid using edges on Γ_D, because the definition conflicts with the essential boundary condition. Thus we make the following modification in the definition of edge paths and $\mathbb{D}_R$:

(1) An edge path connecting two E-boundary components B_1 and B_2 should, if possible, start from $B_1\backslash\Gamma_D$ and end at $B_2\backslash\Gamma_D$.
(2) When one or both of B_1 and B_2 lies in $\mathcal{B}^b$,
   (a) if both B_1 and B_2 are odd E-boundary components, use the edge loop given at the end of Subsection 2.3 to define $\bar{p}(B_1,B_2)$;
   (b) if one of B_1 and B_2 is odd and another is even, use the degenerate edge loop to define $\bar{p}(B_1,B_2)$. The edge attached to the even E-boundary component, in the degenerate edge loop, should not lie in Γ_D. Thus, if the even E-boundary component is in $\mathcal{B}^b$, simply set $\bar{p}(B_1,B_2)=\mathbf{0}$;
   (c) if both B_1 and B_2 are even, then set $\bar{p}(B_1,B_2)=\mathbf{0}$.
(3) The set $\mathbb{D}_R$ is still defined as in (2.9), but with the above modifications and the anchoring E-boundary component B should be chosen as:
   (a) if R is odd, choose an odd E-boundary component as B;
   (b) if R is even and $R\notin\mathcal{R}^b$, choose a B that is not in $\mathcal{B}^b$;
   (c) if R is even and $R\in\mathcal{R}^b$, choose B freely since one will have $dim(\mathscr{D}_R)=0$ anyway, as shown in the next lemma.

Lemma 2.20. *After modification for the Dirichlet boundary* Γ_D*, one has*

$$dim(\mathscr{D}_R)=\begin{cases}0 & \text{for even } R\in\mathcal{R}^b,\\ \#B_{e,R}^i+\#B_{e,R}^m-1 & \text{for even } R\notin\mathcal{R}^b,\\ \#B_{o,R}+\#B_{e,R}^i+\#B_{e,R}^m-2 & \text{for odd } R.\end{cases}$$

It is not hard to see that $dim(\mathscr{D}_R)\ge 0$. Finally, we have

Lemma 2.21. *The cohomology of the cochain complex* (2.13) *satisfies*

$$Ker(\Pi_0^1)/Im(\Pi_0^0)=\bigoplus_{R\in\mathcal{R}}\mathscr{D}_R,$$

and $dim(Ker(\Pi_0^1)/Im(\Pi_0^0))=\#R_e-\sum_{R\in\mathcal{R}}\chi(R)+\#R_e^b-\#B_e^b\ge 0$*, which equals*

$$nullity(\Pi_0^1)-rank(\Pi_0^0)=\left(\#F_e^i-\#T_e+\#R_e^b\right)-\left(\#V_e^i+\sum_{B\in\mathcal{B}}\eta(B)-\#R_e\right).$$

Licensed to AMS.
License or copyright restrictions may apply to redistribution; see https://www.ams.org/journal-terms-of-use

Combining Lemma 2.21 and equation (2.12) gives

Corollary 2.22. *One has*

$$Ker(\Pi_0^1) = \Big(\Pi^0(C_0^0(\mathcal{K})) + \Pi^0(\mathscr{G})\Big) \oplus \Big(\bigoplus_{R\in\mathcal{R}} \mathscr{D}_R\Big).$$

By Lemmas 2.20–2.21 and equation (2.7), one has

Corollary 2.23. *$Ker(\Pi_0^1) = Im(\Pi_0^0)$ if and only if one of the following is true:*

1. *$\#R_e^b = 1$, i.e., the domain Ω is filled with even polygons and $\Gamma_D = \partial\Omega$;*
2. *$\#R_e^b = 0$ and $dim(\mathscr{D}_R) = 0$ for all $R \in \mathcal{R}$, i.e., all odd E-regions have exactly two odd E-boundary components plus any number of $B \in \mathcal{B}_{e,R}^b$, while all even E-regions have exactly one interior/mixed E-boundary component plus any number of $B \in \mathcal{B}_{e,R}^b$.*

Note that $\Pi^0(C_0^0(\mathcal{K})) \subseteq Im(\Pi_0^0) \subseteq Ker(\Pi_0^1)$. The above conditions, plus the condition in Remark 2.18, give the if and only if condition for $Ker(\Pi_0^1) = \Pi^0(C_0^0(\mathcal{K}))$.

2.5. **Global basis functions and the finite element space.** Now we glue the local basis functions together to get global basis functions. Consistent with the definition of the Crouzeix-Raviart finite element space, it is natural to set

$$\begin{aligned} W_h = \{&v \in L^2(\Omega) \text{ such that } v|_T \in Q_T \text{ for all } T \in \mathcal{T} \text{ and} \\ &v \text{ is continuous across midpoints of all } f \in \mathcal{F}\}, \end{aligned} \tag{2.14}$$

$$W_{0,h} = \{v \in W_h \text{ such that } v \text{ vanishes at midpoints of all } f \in \mathcal{F}^b\}.$$

However, such definitions are not useful in practice as the basis functions are not clearly spelled out. We shall examine the structure of W_h and $W_{0,h}$ next.

For simplicity, an extra subscript T is added to the local notation $\mathbf{v}_i$, f_i, $\mathbf{m}_i$, and μ_i defined in Subsection 2.1, to indicate that they are associated with polygon T. For example, $\{\mu_{i,T}\}$ denotes the local basis functions on T.

Define the following set of global functions:

- At each even vertex $\mathbf{v} \in \mathcal{V}_e$, define a basis function $\phi_{\mathbf{v}} \in W_h$ satisfying:
  1. In each even polygon $T \in \mathcal{T}_e$ such that $\mathbf{v}$ is the ith vertex of T, define $\phi_{\mathbf{v}} = \mu_{i,T} \in \hat{Q}_T$. If $\mathbf{v}$ is a phantom of a singular vertex, only the even polygons associated with this phantom are counted.
  2. In $T \in \mathcal{T}_o$ that has $\mathbf{v}$ as a vertex and shares edges with even polygons mentioned in part (1), let $\phi_{\mathbf{v}} \in Q_T$ be the unique function whose values at the midpoints of the shared edges are determined by the values of even neighbors and vanishing at midpoints of all other edges. This is to ensure that $\mathbf{v} \in W_h$.
  3. In all other polygons, set $\phi_{\mathbf{v}} = 0$.
- On each odd edge $f \in \mathcal{F}_o$, noticing that any polygon having f as an edge must be an odd polygon, we define a basis function ϕ_f by:
  1. In an odd polygon T having f as the ith edge, define $\phi_f = \mu_{i,T} \in Q_T$.
  2. In all other polygons, set $\phi_f = 0$.
- In each even polygon $T \in \mathcal{T}_e$, define a basis function $\phi_T = \mu_{0,T}$ in this polygon while vanishing everywhere else.

We introduce spaces spanned by the basis functions defined above:

$$\begin{aligned} Q_h &= span\{\phi_{\mathbf{v}},\, \phi_f,\, \phi_T \text{ for all } \mathbf{v} \in \mathcal{V}_e,\, f \in \mathcal{F}_o,\, T \in \mathcal{T}_e\}, \\ Q_{0,h} &= span\{\phi_{\mathbf{v}},\, \phi_f,\, \phi_T \text{ for all } \mathbf{v} \in \mathcal{V}_e^i,\, f \in \mathcal{F}_o^i,\, T \in \mathcal{T}_e\}. \end{aligned} \tag{2.15}$$

Licensed to AMS.
License or copyright restrictions may apply to redistribution; see https://www.ams.org/journal-terms-of-use

By definition, the spaces Q_h and $Q_{0,h}$ are subspaces of W_h and $W_{0,h}$, respectively. When $\mathcal{T}$ consists of odd polygons only, one clearly has $Q_h = W_h$ and $Q_{0,h} = W_{0,h}$. The identities have also been proved true for quadrilateral meshes in [22, 35]. The proof can easily be extended to meshes consisting of even polygons only.

For general meshes consisting of both odd and even polygons, the situation can be complicated. A discussion about triangular-quadrilateral hybrid meshes is given in [1]. Here we shall give a more comprehensive study of the global finite element spaces, and our study has two important features: (1) we use the cochain complexes (2.8), (2.10), and (2.13) in the analysis; (2) we aim at developing algorithms that automatically deal with complicated mesh structures without human interference.

Using elementary linear algebra, it is clear that

Lemma 2.24. *The finite element spaces satisfy*

$$W_h = \hat{W}_h \oplus \Phi_h, \qquad Q_h = \hat{Q}_h \oplus \Phi_h,$$
$$W_{0,h} = \hat{W}_{0,h} \oplus \Phi_{0,h}, \qquad Q_{0,h} = \hat{Q}_{0,h} \oplus \Phi_{0,h},$$

where

$$\begin{aligned} \hat{W}_h &= \{v \in W_h \text{ such that } v|_T \in \hat{Q}_T \text{ for all } T \in \mathcal{T}_e \text{ and} \\ &\qquad v \text{ vanishes at midpoints of all } f \in \mathcal{F}_o\}, \\ \hat{Q}_h &= span\{\phi_{\mathbf{v}} \text{ for all } \mathbf{v} \in \mathcal{V}_e\}, \\ \Phi_h &= span\{\phi_f, \phi_T \text{ for all } f \in \mathcal{F}_o, T \in \mathcal{T}_e\}, \end{aligned} \tag{2.16}$$

and

$$\begin{aligned} \hat{W}_{0,h} &= \{v \in \hat{W}_h \text{ such that } v \text{ vanishes at midpoints of all } f \in \mathcal{F}^b\}, \\ \hat{Q}_{0,h} &= span\{\phi_{\mathbf{v}} \text{ for all } \mathbf{v} \in \mathcal{V}_e^i\}, \\ \Phi_{0,h} &= span\{\phi_f, \phi_T \text{ for all } f \in \mathcal{F}_o^i, T \in \mathcal{T}_e\}. \end{aligned} \tag{2.17}$$

Proof. The decompositions for Q_h and $Q_{0,h}$ are straightforward. For each $v \in W_h$ or $W_{0,h}$, its decomposition in $\hat{W}_h \oplus \Phi_h$ or $\hat{W}_{0,h} \oplus \Phi_{0,h}$ can be explicitly constructed. The decomposition is a direct sum since each function in the spanning set of Φ_h is linearly independent from $\hat{W}_h$. □

It is clear that $\hat{Q}_h \subseteq \hat{W}_h$ and $\hat{Q}_{0,h} \subseteq \hat{W}_{0,h}$. Now we state an important relation between the finite element spaces and the cochain complexes (2.8), (2.10), and (2.13). Define a map $\iota : \hat{W}_h \to C^1(\mathcal{K})$ by taking the value of functions at midpoints of even edges, i.e.,

> Given $v \in \hat{W}_h$, for each even edge $f \in \mathcal{F}_e$, the entry of vector $\iota(v) \in C^1(\mathcal{K})$ associated with f is equal to $v(\mathbf{m}_f)$, where $\mathbf{m}_f$ denotes the midpoint of edge f.

Lemma 2.25. *The linear spaces $\hat{W}_h$ and $\hat{Q}_h$ are isomorphic to $Ker(\Pi^1)$ and $Im(\Pi^0)$, respectively, under the map ι. Similarly, spaces $\hat{W}_{0,h}$ and $\hat{Q}_{0,h}$ are isomorphic to $Ker(\Pi_0^1)$ and $\Pi_0^0(C_0^0(\mathcal{K}))$, respectively, under ι.*

Proof. Note that ι is linear. It is obvious that $Ker(\iota) = \{0\}$. By Remark 2.2 and noticing that the rows of Π^1 are just the constraints (2.3) on all $T \in \mathcal{T}_e$, one immediately has $\iota(\hat{W}_h) = Ker(\Pi^1)$. Since all spaces are finite dimensional, it is clear that ι is an isomorphism from $\hat{W}_h$ to $Ker(\Pi^1)$.

Licensed to AMS.
License or copyright restrictions may apply to redistribution; see https://www.ams.org/journal-terms-of-use

For $\hat{Q}_h$, we first note that every function $v \in \hat{Q}_h$ can be expressed as $v = \sum_{\mathbf{v}\in\mathcal{V}_e} v_{\mathbf{v}}\phi_{\mathbf{v}}$, where the $v_{\mathbf{v}}$'s are the coefficients of the linear combination. The coefficients $v_{\mathbf{v}}$ for all $\mathbf{v} \in \mathcal{V}_e$ form the entries of a vector, denoted by $[v_{\mathbf{v}}]$, in $C^0(\mathcal{K})$. By the definition of $\phi_{\mathbf{v}}$, the value of function v at the midpoint of each $f \in \mathcal{F}_e$ is just the summation of coefficients $v_{\mathbf{v}}$ associated with the two ends of the edge f, i.e.,

$$\iota(v) = \Pi^0[v_{\mathbf{v}}].$$

Conversely, for any given vector in $C^0(\mathcal{K})$, one can easily construct a function $v \in \hat{Q}_h$ by setting $[v_{\mathbf{v}}]$ equal to the given vector. Thus $\hat{Q}_h$ is isomorphic to $Im(\Pi^0)$ under the map ι.

The proof for $\hat{W}_{0,h}$ and $\hat{Q}_{0,h}$ is similar. □

Remark 2.26. Note that $\hat{Q}_{0,h}$ is isomorphic to $\Pi_0^0(C_0^0(\mathcal{K}))$, which may be smaller than $Im(\Pi_0^0) = \Pi_0^0(\tilde{C}_0^0(\mathcal{K}))$.

Remark 2.27. Combining Lemma 2.25 and Lemma 2.13, we have

$$\hat{W}_h = \hat{Q}_h \oplus \iota^{-1}\left(\bigoplus_{R\in\mathcal{R}} \mathscr{D}_R\right)$$

and $dim(\hat{W}_h) = nullity(\Pi^1) = \#F_e - \#T_e$. Similarly, combining Lemma 2.25 and Corollary 2.22, we have

$$\hat{W}_{0,h} = \left(\hat{Q}_{0,h} + \iota^{-1}\Pi^0(\mathscr{G})\right) \oplus \iota^{-1}\left(\bigoplus_{R\in\mathcal{R}} \mathscr{D}_R\right)$$

and $dim(\hat{W}_{0,h}) = nullity(\Pi_0^1) = \#F_e^i - \#T_e + \#R_e^b$.

The structures of spaces W_h, Q_h, $W_{0,h}$, and $Q_{0,h}$ become clear after Lemmas 2.24–2.25. One has two ways to define global nonconforming finite element spaces:

Method 1: Use Q_h or $Q_{0,h}$ as the global finite element space.

- A spanning set is given in (2.15), which provides "global basis functions".
- By Lemma 2.25, Lemma 2.10, and Corollary 2.17,

$$dim(\hat{Q}_h) = rank(\Pi^0) = \#V_e - \#R_e,$$
$$dim(\hat{Q}_{0,h}) = dim(\Pi_0^0(C_0^0(\mathcal{K}))) = \#V_e^i - \#R_e^i.$$

  Thus the spanning set for Q_h or $\hat{Q}_{0,h}$ is linearly dependent when $\#R_e > 0$ or $\#R_e^i > 0$, respectively.
- Thanks to the analysis from Subsections 2.3–2.4, we do know how to make the spanning set linearly independent when constructing $\phi_{\mathbf{v}}$'s (note that the ϕ_f and ϕ_T parts are already linearly independent). One just needs to skip an even vertex (any one will do) for each $R \in \mathcal{R}_e$ in case of pure Neumann boundary problems (see Lemma 2.10 and Lemma 2.25), or to skip an even vertex for each $R \in \mathcal{R}_e^i$ in case of problems with Dirichlet boundaries (see Corollary 2.17 and Lemma 2.25). This, although it can be done by computer codes automatically, causes extra trouble in the implementation as one has to develop a programming module for recognizing all even E-regions. We point out

Licensed to AMS.
License or copyright restrictions may apply to redistribution; see https://www.ams.org/journal-terms-of-use

that, for linear problems, it is indeed fine to leave the spanning set linearly dependent, as will be explained later in this subsection.

Method 2: Use W_h or $W_{0,h}$ as the global finite element space.

- The space W_h is spanned by, due to Lemmas 2.24–2.25 and Remark 2.27,

$$\{\phi_{\mathbf{v}},\ \phi_f,\ \phi_T \text{ for all } \mathbf{v} \in \mathcal{V}_e,\ f \in \mathcal{F}_o,\ T \in \mathcal{T}_e,$$
$$\text{and functions in } \iota^{-1}(\mathbb{D}_R) \text{ for all } R \in \mathcal{R}\},$$

  where $\mathbb{D}_R$ is a spanning set for $\mathscr{D}_R$ as defined in (2.9). The spanning set may be linearly dependent, but can in many cases still be used as "global basis functions" for W_h. Similar to Method 1, we do know how to make the basis functions linearly independent.
- Similarly, the space $W_{0,h}$ is spanned by

$$\{\phi_{\mathbf{v}},\ \phi_f,\ \phi_T \text{ for all } \mathbf{v} \in \mathcal{V}_e^i,\ f \in \mathcal{F}_o^i,\ T \in \mathcal{T}_e,$$
$$\text{functions in } \iota^{-1}(\mathbb{D}_R) \text{ for all } R \in \mathcal{R},$$
$$\text{and functions in } \iota^{-1}\Pi^0(\mathbb{G}_B) \text{ for all } B \in \mathcal{B}_e^b \cup \mathcal{B}^m\},$$

  where $\mathbb{G}_B$ is a spanning set for $\mathscr{G}_B$ as defined in (2.11). Again, the spanning set may be linearly dependent. But using the analysis from Subsections 2.3–2.4, we do know which basis functions to drop in order to make the rest linearly independent.

Remark 2.28. Corollary 2.14 states the condition for $Q_h = W_h$. Remark 2.18 plus Corollary 2.23 state the condition for $Q_{0,h} = W_{0,h}$. Methods 1 and 2 are different otherwise.

Now we explain why the linear dependency of spanning sets in spaces W_h, Q_h, $W_{0,h}$, and $Q_{0,h}$ does not cause much trouble in actual implementation, assuming one is solving a linear differential equation. For example, consider the finite element approximation: Find $u_h \in Q_{0,h}$ such that $a(u_h, \phi) = b(\phi)$ for all $\phi \in Q_{0,h}$, where $a(\cdot,\cdot)$ and $b(\cdot)$ are the bilinear form and the linear form, respectively. This leads to a linear system $A\mathbf{x} = \mathbf{b}$, where A is the stiffness matrix and $\mathbf{b}$ is the right-hand side vector. It is not hard to see that the kernel of matrix A contains only vectors corresponding to $\phi \equiv 0$, i.e., vectors from $Ker(\Pi_0^0)$. Such vectors will set the right-hand side $b(\phi) = b(0) = 0$, i.e., $\mathbf{b}$ is orthogonal to these vectors. Therefore the linear system is consistent and a modern linear solver can easily handle such a situation. In Section 4, numerical results will be given, which further verify this observation.

Finally, we mention that the H^1-conforming finite element spaces built by Q_T,

$$U_h = \{v \text{ is continuous in } \Omega \text{ and satisfies } v|_T \in Q_T \text{ for all } T \in \mathcal{T}\},$$
$$U_{0,h} = \{v \in U_h \text{ such that } v|_{\Gamma_D} = 0\},$$

are subspaces of Q_h and $Q_{0,h}$, respectively.

Lemma 2.29. *One has $U_h \subseteq Q_h$ and $U_{0,h} \subseteq Q_{0,h}$.*

Proof. Let $w \in U_h$. Define

$$\psi = \sum_{\mathbf{v} \in \mathcal{V}_e} \frac{w(\mathbf{v})}{2}\phi_{\mathbf{v}} + \sum_{f \in \mathcal{F}_o} w(\mathbf{m}_f)\phi_f + \sum_{T \in \mathcal{T}_e} w_T \phi_T \in Q_h,$$

Licensed to AMS.
License or copyright restrictions may apply to redistribution; see https://www.ams.org/journal-terms-of-use

where $\mathbf{m}_f$ denotes the midpoint of edge f, and w_T is defined in each $T \in \mathcal{T}_e$ with local vertices $\mathbf{v}_{1,T}, \ldots, \mathbf{v}_{n,T}$ by

$$w_T = \frac{1}{n}\Big(w(\mathbf{v}_{1,T}) - w(\mathbf{v}_{2,T}) + w(\mathbf{v}_{3,T}) - w(\mathbf{v}_{4,T}) + \cdots - w(\mathbf{v}_{n,T})\Big).$$

We shall show that $\psi \equiv w$ and consequently one has $U_h \subseteq Q_h$. Indeed, in each even polygon T, one has

$$\begin{aligned}\psi|_T &= \sum_{i=1}^{n} \frac{w(\mathbf{v}_{i,T})}{2}\mu_{i,T} + w_T\mu_{0,T} \\ &= \sum_{i=1}^{n} w(\mathbf{v}_{i,T})\Big(\lambda_{i,T} + \frac{(-1)^i}{n}\mu_{0,T}\Big) + w_T\mu_{0,T} \\ &= \sum_{i=1}^{n} w(\mathbf{v}_{i,T})\lambda_{i,T} = w|_T.\end{aligned}$$

In each odd polygon, note that by definition

$$\psi(\mathbf{m}_{i,T}) = \begin{cases} w(\mathbf{m}_{i,T}) & \text{if } f_{i,T} \in \mathcal{E}_o, \\ \frac{w(\mathbf{v}_{i,T})}{2} + \frac{w(\mathbf{v}_{i+1,T})}{2} = w(\mathbf{m}_{i,T}) & \text{if } f_{i,T} \in \mathcal{E}_e. \end{cases}$$

Thus by Lemma 2.1, one must have $\psi|_T \equiv w|_T$ in odd polygons too. This completes the proof for $U_h \subseteq Q_h$. The proof of $U_{0,h} \subseteq Q_{0,h}$ is similar. □

3. Error analysis

In this section, we discuss the approximation error of the nonconforming finite element method for solving Poisson equations with homogeneous Dirichlet boundary condition. The analysis can easily be extended to general second order elliptic equations with other types of boundary conditions. Consider the example problem in its variational form: Find $u \in H_0^1(\Omega)$ satisfying

$$(\nabla u, \nabla v) = b(v) \quad \text{for all } v \in H_0^1(\Omega), \tag{3.1}$$

where $(\cdot,\cdot)$ denotes the L^2 innerproduct over Ω and $b(\cdot) \in H^{-1}(\Omega)$. Let $\mathcal{T}$ be a polygonal mesh on Ω and denote by ∇_h the piecewisely-defined gradient operator on $\mathcal{T}$. Then one may consider the nonconforming finite element approximation either in the space $Q_{0,h}$ or in $W_{0,h}$: Find $u_h \in Q_{0,h}$ (or $W_{0,h}$) satisfying

$$(\nabla_h u_h, \nabla_h v) = b(v) \quad \text{for all } v \in Q_{0,h} \text{ (or } W_{0,h}). \tag{3.2}$$

In the rest of this section, we shall only discuss the case when the finite element space is set to $Q_{0,h}$. The analysis for $W_{0,h}$ is exactly the same.

Note that $(\nabla_h \cdot, \nabla_h \cdot)$ is an innerproduct on $Q_{0,h}$ since $(\nabla_h v, \nabla_h v) = 0$ implies that v be piecewise-constant on the mesh $\mathcal{T}$. Using the continuity across midpoints of interior edges and the fact that v vanishes at midpoints of boundary edges, one immediately gets $v \equiv 0$. Thus $(\nabla_h \cdot, \nabla_h \cdot)$ is an innerproduct and consequently the nonconforming finite element problem admits a unique solution.

For convenience, Sobolev norms and seminorms on $H^s(K)$, for $s = 0, 1, 2$ and K any given domain, are denoted by $\|\cdot\|_{s,K}$ and $|\cdot|_{s,K}$, respectively. Define the broken energy norm in $Q_{0,h}$ by

$$\|v\|_h = (\nabla_h v, \nabla_h v)^{1/2}.$$

Licensed to AMS.
License or copyright restrictions may apply to redistribution; see https://www.ams.org/journal-terms-of-use

We use $\lesssim$ to denote "less than or equal to up to a general constant independent of the mesh size".

Before presenting the error analysis, we need to discuss mesh regularity conditions. It is well known that finite element meshes should satisfy certain regularity conditions in order for the approximation to achieve optimal a priori error estimates. While regularity conditions for triangular meshes are well known [8], there are only a few recent works on regularity for polygonal meshes [5, 11, 17, 19, 33, 42], among which [17] and [19] consider mesh regularity for generalized barycentric coordinates (nonpolynomial) and all others only consider piecewise polynomial discrete spaces. Denote by h_T the diameter of polygon $T \in \mathcal{T}$. Following [17, 19], we assume the following.

Mesh regularity assumption. For all polygons in mesh $\mathcal{T}$:

- The area of the polygon satisfies $|T| \approx h_T^2$.
- The gradient of each GBC in $\{\lambda_{i,T}\}$ satisfies $|\nabla \lambda_i| \lesssim h_T^{-1}$ at all $\mathbf{x} \in T$, where $|\cdot|$ stands for the Euclidean length. This has been proved true in [17] for the Wachspress coordinates as long as h^*, the minimum distance from any vertex of T to a nonincidental edge, satisfies $h^* \approx h_T$.
- The following trace inequality and the approximation property of L^2 projection are true:

$$\begin{aligned} &\|\phi\|^2_{L^2(\partial T)} \lesssim h_T^{-1}\|\phi\|_T^2 + h_T\|\nabla\phi\|_T^2 && \text{for } \phi \in H^1(T), \\ &\|\phi - \frac{1}{|T|}\int_T \phi\, dx\|_T \lesssim h_T\|\phi\|_{1,T} && \text{for } \phi \in H^1(T). \end{aligned} \tag{3.3}$$

It is known that when T satisfies certain shape regularity conditions [5, 11, 33, 42], inequality (3.3) holds on T.

Now we start the error analysis. By the second Strang's Lemma, one has

$$\|u - u_h\|_h \lesssim \inf_{v \in Q_{0,h}} \|u - v\|_h + \sup_{w \in Q_{0,h}\setminus\{0\}} \frac{(\nabla_h(u - u_h), \nabla_h w)}{\|w\|_h}, \tag{3.4}$$

where the right-hand side of the inequality consists of the interpolation error and the consistency error. An upper bound of the interpolation error follows immediately from Lemma 2.29 and the interpolation error of the H^1-conforming finite element space $U_{0,h}$ on polygonal meshes [17, 19], under assumed mesh regularity:

$$\inf_{v \in Q_{0,h}} \|u - v\|_h \le \inf_{v \in U_{0,h}} \|u - v\|_h \lesssim \left(\sum_{T \in \mathcal{T}} h_T^2 |u|^2_{2,T}\right)^{1/2}. \tag{3.5}$$

Estimation of the consistency error is also standard. For all $w \in Q_{0,h}$, one has

$$\begin{aligned} (\nabla_h(u - u_h), \nabla_h w) &= \sum_{T \in \mathcal{T}} \Big(\int_{\partial T} \nabla u \cdot (w\mathbf{n})\, ds - (\Delta u, w)\Big) - (\nabla_h u_h, \nabla_h w) \\ &= \sum_{f \in \mathcal{F}} \int_f \nabla u \cdot [\![w]\!]\, ds, \end{aligned}$$

where the jump term $[\![w]\!]$ on edge f is defined by

$$[\![w]\!] = \begin{cases} w|_{T_1}\mathbf{n}_1 + w|_{T_2}\mathbf{n}_2 & \text{if } f \text{ is an interior edge shared by polygons } T_1, T_2, \\ w|_T \mathbf{n} & \text{if } f \text{ is on } \partial\Omega \cap \partial T, \end{cases}$$

Licensed to AMS.
License or copyright restrictions may apply to redistribution; see https://www.ams.org/journal-terms-of-use

in which $\mathbf{n}_1$, $\mathbf{n}_2$, and $\mathbf{n}$ are the unit outward normal vectors on f, with respect to T_1, T_2, and T, respectively. Note that $[\![w]\!]$ vanishes at the center of edge f. On each edge f, assign a fixed unit normal direction denoted by $\mathbf{n}_f$ and let $c_f = \frac{1}{|f|}\int_f \nabla u \cdot \mathbf{n}_f \, ds$, where $|f|$ is the length of f. That is, c_f is the L^2 projection of $\nabla u \cdot \mathbf{n}_f$. By (3.3) and noticing that $\|\nabla u \cdot \mathbf{n}_f - c_f\|_{0,f} \le \|\nabla u \cdot \mathbf{n}_f - c\|_{0,f}$ for any constant c, one gets

$$\begin{aligned}\sum_{f\in\mathcal{F}}\int_f \nabla u\cdot[\![w]\!]\,ds &= \sum_{f\in\mathcal{F}}\int_f (\nabla u\cdot\mathbf{n}_f - c_f)\mathbf{n}_f\cdot[\![w]\!]\,ds\\ &\le \Big(\sum_{f\in\mathcal{F}}|f|\|\nabla u\cdot\mathbf{n}_f - c_f\|_{0,f}^2\Big)^{1/2}\Big(\sum_{f\in\mathcal{F}}|f|^{-1}\|[\![w]\!]\|_{0,f}^2\Big)^{1/2}\\ &\lesssim \Big(\sum_{T\in\mathcal{T}} h_T^2|u|_{2,T}^2\Big)^{1/2}\|w\|_h,\end{aligned}$$

while in the last step the estimate for $\|[\![w]\!]\|_{0,f}$ follows from the fact that $[\![w]\!]$ vanishes at the midpoint of edges. Combining the above, we get the consistency error

$$\frac{(\nabla_h(u-u_h),\,\nabla_h w)}{\|w\|_h} \lesssim \Big(\sum_{T\in\mathcal{T}} h_T^2|u|_{2,T}^2\Big)^{1/2}. \tag{3.6}$$

Finally, by equations (3.4), (3.5), and (3.6), one gets:

Theorem 3.1. *Let u and u_h be the solution to problems* (3.1) *and* (3.2)*, respectively, and assume that $\mathcal{T}$ satisfies the mesh regularity assumptions. Then one has*

$$\|u-u_h\|_h \lesssim \Big(\sum_{T\in\mathcal{T}} h_T^2|u|_{2,T}^2\Big)^{1/2}.$$

Remark 3.2. An optimal L^2 error estimate can similarly be derived. We omit the details as it is just another routine work.

Remark 3.3. The optimal error estimates can be extended straightforwardly to $W_{0,h}$ or to the cases of Neumann boundary conditions. But so far we do not know whether the subtle difference between spaces $Q_{0,h}$ and $W_{0,h}$, or between spaces Q_h and W_h, will have an impact on numerical simulation of certain physical problems or not.

4. Implementation and numerical results

4.1. **Implementation.** The nonconforming method using the space Q_h or $Q_{0,h}$ can be implemented easily, which will be discussed in this section. If one prefers to use the space W_h or $W_{0,h}$, extra efforts are needed in order to add functions in $\mathbb{D}_R$ and $\mathbb{G}_B$. Since both methods provide optimal a priori error, we focus on the easy one using Q_h or $Q_{0,h}$.

The implementation follows the usual finite element framework, i.e., compute the local stiffness matrices/right-hand sides and then assemble the global matrix/right-hand side. Comparing to the implementation of the conforming finite element method based on generalized barycentric coordinates, one only needs to add three simple extra steps in the algorithm. (1) In the given mesh, mark even/odd polygons, vertices and edges. (2) On each polygon T, fill a simple transfer matrix C_T. Then

Licensed to AMS.
License or copyright restrictions may apply to redistribution; see https://www.ams.org/journal-terms-of-use

the local stiffness matrix of the nonconforming method is just $C_T A_T C_T^t$, where A_T denotes the local stiffness matrix of the conforming finite element method using GBC. And the local right-hand side is $C_T \mathbf{b}_T$, where $\mathbf{b}_T$ is the local right-hand side of the conforming finite element method. (3) Before the assembling stage, a data structure containing information about phantom vertices should be built.

Next we give detailed algorithms for these three steps.

Algorithm 1. *For marking even/odd polygons, vertices, and edges:*

(1) *Initializing: mark all polygons, edges, vertices* odd.
(2) *For each $T \in \mathcal{T}$: if T is even, mark T and all its edges, vertices* even.

Algorithm 2. *For computing the local stiffness matrix and the right-hand side vector:*

(1) *On polygon T, compute matrix $A_T = [a(\lambda_{j,T}, \lambda_{i,T})]_{1\le i,j\le n}$ and vector $\mathbf{b}_T = [F(\lambda_{i,T})]_{1\le i\le n}$, which are the same as the local stiffness matrix and the right-hand side for the conforming finite element method using generalized barycentric coordinates. One can use available code from, for example,* [17] *for the Wachspress element.*
(2) *For odd polygons, simply set the transfer matrix $C_T = B$ with B given in* (2.4)*; for even polygons, set*

$$C_T = \begin{bmatrix} \overline{a}_T^t \\ D \end{bmatrix},$$

where vector $\overline{a}_T$ and matrix D are defined as in (2.2) *and* (2.6)*, respectively. Then the local stiffness matrix and the right-hand side for the nonconforming method are just $C_T A_T C_T^t$ and $C_T \mathbf{b}_T$.*

Algorithm 3. *For building data structure of phantoms:*

(1) *Define an interior edge to be a "switcher" if it is shared by an odd polygon and an even polygon. Run through all interior edges to mark the switchers.*
(2) *For every even vertex $\mathbf{v}$, define its "switcher count" $s(\mathbf{v})$ by: if $\mathbf{v} \notin \partial\Omega$, then $s(\mathbf{v})$ is the number of switchers connected to $\mathbf{v}$; if $\mathbf{v} \in \partial\Omega$, then $s(\mathbf{v})$ is the number of switchers plus the number of even edges on $\partial\Omega$ that have $\mathbf{v}$ as an end. An illustration is given in Figure* 7*, which shows that $\frac{s(\mathbf{v})}{2}$ is exactly the number of even regions attached to $\mathbf{v}$, i.e., the number of phantoms that $\mathbf{v}$ should be split into. Thus $\mathbf{v}$ is singular if and only if $s(\mathbf{v}) > 2$. Run through all even vertices to mark singular ones and their phantom counts.*
(3) *For each singular vertex, sort all edges, starting from a switcher, connected to the vertex counterclockwisely. This can be done through sorting the polar angle of edge vectors. Then, polygons surrounding the singular vertex are divided, in counterclockwise order, into (even-odd-even-...) or (odd-even-odd-...) blocks by the switchers. Assign a phantom to each even block. For each polygon in this even block, redirect its vertex pointer such that it points to the phantom instead of the physical even vertex.*

Remark 4.1. For meshes with the half-edge data structure [10, 24, 31], Algorithm 3 is not needed as the same functionality can be easily implemented through the half-edge structure. Algorithm 3 is designed for meshes with only polygon-to-vertex, polygon-to-edge, and edge-to-polygon maps.

Licensed to AMS.
License or copyright restrictions may apply to redistribution; see https://www.ams.org/journal-terms-of-use

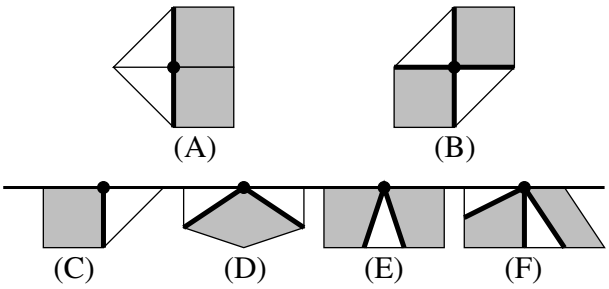

FIGURE 7. Even vertices and switchers. Vertex $\mathbf{v}$ is denoted by a solid dot, even polygons are marked in gray, and switchers are marked in thick lines. The long line in the second row denotes $\partial\Omega$. (A) An interior even vertex with $s(\mathbf{v}) = 2$; (B) an interior even vertex with $s(\mathbf{v}) = 4$; (C)–(D) even vertices on $\partial\Omega$ with $s(\mathbf{v}) = 2$; (E)–(F) even vertices on $\partial\Omega$ with $s(\mathbf{v}) = 4$. Vertices in (A), (C), (D) are nonsingular and the rest are singular.

4.2. **Numerical Test 1.** The first test focuses on the asymptotic order of the H^1 seminorm and the L^2 norm of the approximation error. Consider the Poisson equation on $\Omega = (0,1) \times (0,1)$ with the Dirichlet boundary condition. We test this problem on three different types of meshes, as shown in Figure 8. The Wachspress coordinates are used to define λ_i. The example problem is solved on a sequence of meshes with characteristic mesh size h varying. We first set the exact solution to be $u = \sin(2\pi x)\sin(2\pi y)$, which is smooth, and then test the problem with exact solution $u = \sqrt{\frac{1}{2}(\rho - x) - \frac{1}{4}\rho^2}$, where ρ is the radius in polar coordinates. The second example has a corner singularity. It is well known that one should expect optimal convergence rates for the smooth example and $h^{1/2}$ order less for the corner singularity example. For simplicity, the error $I_h u - u_h$, where I_h is the nodal value interpolation, is computed instead of $u - u_h$. Numerical results are reported in Figure 9. From the figures we can see that $\|I_h u - u_h\|_{L^2}$ and $|I_h u - u_h|_{H^1}$ agree well with the theoretical predictions for meshes of type (A) and (B). For type (C) meshes, the convergence rate degenerates a little, which we suspect is caused by the combined effect of deteriorating mesh regularity and bad quality of the stiffness matrix.

4.3. **Numerical Test 2.** The second test focuses on the effect of the nullspace of the stiffness matrix. By Lemmas 2.16 and 2.25, we know that the stiffness matrix A may have a nontrivial nullspace. In extreme situations when $\#R_e$ or $\#R_e^i$ is large, this nullspace can be quite large, i.e., the nullity of the matrix A is large. We have already explained in Subsection 2.5 that, (1) the analysis from Subsections 2.3–2.4 does tell us exactly how many and which basis functions to drop in order to make the rest linearly independent, i.e., to make A nonsingular; (2) for linear differential equations, such nullspace does not affect the consistency of the linear system to be solved, and modern iterative solvers are able to handle this, if carefully designed. Here we test, in the latter case, how well the Matlab built-in direct solver can handle this situation.

Licensed to AMS.
License or copyright restrictions may apply to redistribution; see https://www.ams.org/journal-terms-of-use

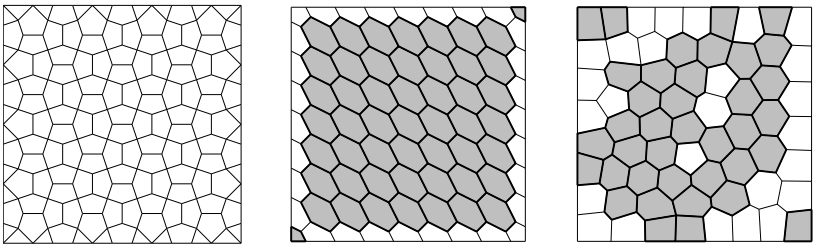

FIGURE 8. Polygonal meshes for Test 1. Even polygons are marked with gray. (A) Cairo tiling modified on the boundary. This mesh contains only odd polygons. (B) A mesh consists of mostly hexagons. (C) Random quasi-centroidal Voronoi tessellation.

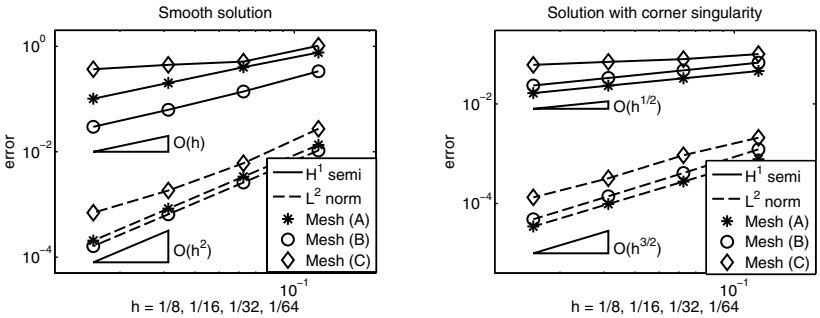

FIGURE 9. Approximation error for Test 1 on three types of meshes. H^1 seminorm is $|I_h u - u_h|_{H^1}$ and L^2 norm is $\|I_h u - u_h\|_{L^2}$.

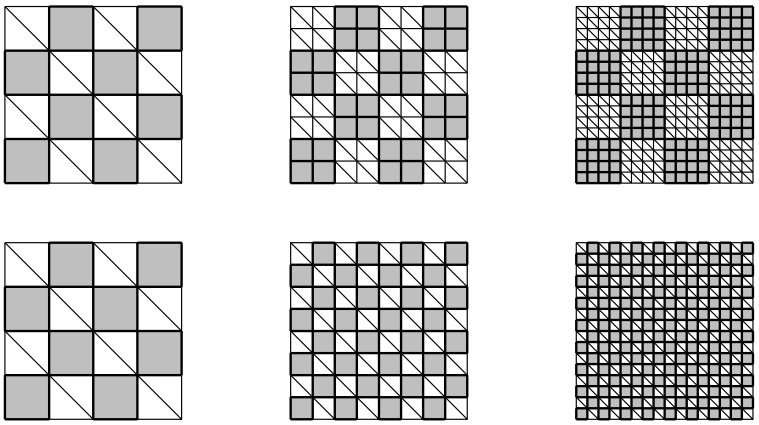

FIGURE 10. Meshes for Test 2.

Consider two types of mesh families shown in Figure 10. The first row contains meshes with fixed $\#\mathcal{R}$ during the uniform refinement. For meshes in this family

Licensed to AMS.
License or copyright restrictions may apply to redistribution; see https://www.ams.org/journal-terms-of-use

TABLE 1. Convergence of Test 2.

	Case 1		Case 2		Case 3	
h	H^1 semi	L^2	H^1 semi	L^2	H^1 semi	L^2
1/4	–	–	–	–	2.70e+00	1.95e-01
1/8	1.47e+00	5.35e-02	1.53e+00	5.71e-02	1.53e+00	5.71e-02
1/16	7.46e-01	1.35e-02	–	–	7.77e-01	1.49e-02
1/32	3.73e-01	3.37e-03	3.88e-01	3.76e-03	3.88e-01	3.76e-03
1/64	1.86e-01	8.38e-04	–	–	1.94e-01	9.41e-04
$O(h^r), r =$	0.99	2.00	0.99	1.96	0.99	1.98

the nullity of the stiffness matrix does not change when h decreases. The second row contains meshes with an increasing $\#\mathcal{R}$, and the nullity of stiffness matrix will increase when h decreases.

We solve the Poisson equation with the Dirichlet boundary condition on these two families of meshes, and set the exact solution $u = \sin(2\pi x)\sin(2\pi y)$. The test is divided into three cases:

- Case 1. Solve the problem using meshes in row 1 of Figure 10, leaving the nullity of the stiffness matrix to be dealt with by the linear solver.
- Case 2. Solve the problem using meshes in row 2 of Figure 10, leaving the nullity of the stiffness matrix to be dealt with by the linear solver.
- Case 3. Again we use meshes in row 2 of Figure 10. But we drop, for each interior E-region, a basis function associated with a random even vertex. This, according to the analysis given in Subsection 2.5, is the minimum action in order to make the rest of the basis functions linearly independent, i.e., to make the stiffness matrix nonsingular. The nonsingularity of the stiffness matrix has also been confirmed by computing $rank(A)$ in Matlab.

Numerical results of $\|I_h u - u_h\|_{L^2}$ and $|I_h u - u_h|_{H^1}$ are reported in Table 1. In Case 1, the direct solver fails for $h = 1/4$ but works fine for finer meshes and gives the correct asymptotic order of the error. In Case 2, it seems the large nullity has put stress on the direct solver, which fails for $h = 1/4$, $1/16$, and $1/64$. Case 3 is the most stable one since the stiffness matrix is nonsingular in this case. Interestingly, we notice that for $h = 1/8$ and $1/32$, the solutions for Case 2 and Case 3 are exactly the same. This is not hard to understand, as Case 2 and Case 3 are essentially the same problem, while the stiffness matrix in Case 3 is a "compact" version of the stiffness matrix in Case 2. In general, we expect that the Krylov subspace iterative methods should perform better than the Matlab built-in direct solver in handling the large kernel of stiffness matrices.

4.4. **Numerical Test 3.** Recall that the local basis function μ_0 defined in (2.1) for even polygons can be considered as a "bubble function" as it vanishes at midpoints of all edges of an even polygon. In the theoretical analysis, so far we are not able to drop μ_0 in the nonconforming method since it is not clear whether $\hat{Q}_T$ contains the entire P_1 or not. However, this can be easily checked numerically. Test 3 is designed for this purpose.

Licensed to AMS.
License or copyright restrictions may apply to redistribution; see https://www.ams.org/journal-terms-of-use

Again we solve the Poisson equation with exact solution $u = \sin(2\pi x)\sin(2\pi y)$. Meshes of types (B) and (C), as shown in Figure 8, are used. We call the original nonconforming finite element method a "full" method, and define a "reduced" method by using the same construction but without the basis function μ_0 on even polygons. Numerical results are reported in Figure 11.

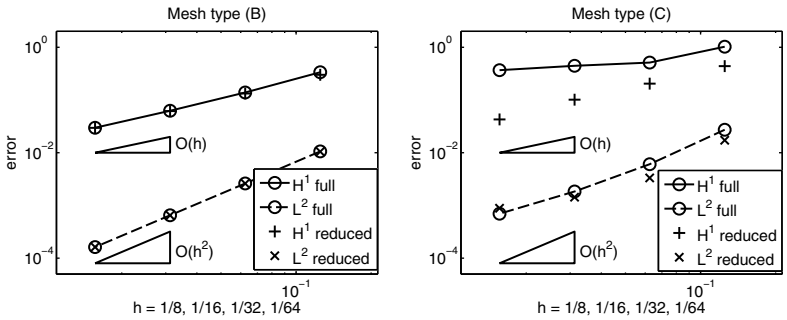

FIGURE 11. Approximation error with or without μ_0.

For meshes of type (B), solutions for the full method and the reduced method are almost identical, as shown in the left graph of Figure 11. The numbers are indeed different but the difference is too small to be discernible in the graph. It is interesting to see that dropping μ_0 does not seem to affect the approximation error at all. So far we are not able to explain this in the theory. For meshes of type (C), results from the reduced method are even better, which we suspect is due to the better quality of the stiffness matrix, but we cannot yet confirm it.

APPENDIX A. PROOF OF LEMMAS IN SECTION 2.3

Proof of Lemma 2.9. All entries of a vector in $\mathscr{A}_R$ are completely determined by one number and thus $dim(\mathscr{A}_R) \leq 1$. For odd E-regions, by examining the entries associated with vertices on an odd E-boundary component, one immediately sees that the alternating pattern cannot exist and hence $dim(\mathscr{A}_R) = 0$. Next, consider even E-regions. We start from the case when R is simply connected. If R contains only one even polygon, then alternating vectors can be explicitly constructed and $dim(\mathscr{A}_R) = 1$. Expand R by gluing new even polygons to it one by one, and expand the alternating vector accordingly. The glued polygons can be viewed as a larger even polygon, by erasing interior edges. Thus by induction one has $dim(\mathscr{A}_R) = 1$. This process can easily be extended to even E-regions that are not simply connected, noticing that each "hole" in such E-region can also be viewed and glued as an even polygon. This completes the proof of the lemma. □

Proof of Lemma 2.10. The direct sum is obvious since E-regions are completely disjoint after the introduction of phantoms. It is clear that $\mathscr{A}_R \subseteq Ker(\Pi^0)$. On the other hand, let $\bar{c}^0 \in Ker(\Pi^0)$. If the entry of $\bar{c}^0$ at an even vertex is nonzero, by the definition of Π^0, the entries of $\bar{c}^0$ at surrounding even vertices are immediately determined. Then, this expands further out until all entries on this E-region are determined. Again by the definition of Π^0, the entries must form an alternating pattern. This completes the proof of $Ker(\Pi^0) = \bigoplus_{R\in\mathcal{R}_e} \mathscr{A}_R$. The calculation of nullity and rank for Π^0 is elementary. □

Licensed to AMS.
License or copyright restrictions may apply to redistribution; see https://www.ams.org/journal-terms-of-use

Proof of Lemma 2.11. By the rank-nullity relation, one only needs to show that the rows of matrix Π^1 are linearly independent. Such kind of proof was first given in [35] for quadrilateral meshes. Its extension to an even submesh is straightforward. For the reader's convenience, we briefly state the idea. Note that each row of Π^1 corresponds to one even polygon. For any set of rows whose linear combination is zero, mark the corresponding even polygons. The marked set must have boundary. In a column of Π^1 corresponding to an edge on this boundary, only one row(polygon) in the marked row(polygon) set has a nonzero entry on this column(edge). Thus the coefficient of this row in the linear combination must be 0. Repeat the process until all coefficients in the linear combination become 0. This indicates that all rows are linearly independent. □

Proof of Lemma 2.12. The spanning set $\mathbb{D}_R$ contains exactly $\#B_R - 1$ vectors. We point out that when at least one of B and B' is even, then $\overline{p}(B, B') \notin Im(\Pi^0)$. Indeed, by viewing the even boundary component as the boundary of an even polygon, vector $\overline{p}(B, B')$ violates rule (2.3) in that even polygon, which means it cannot be generated by nodal values using Π^0. Now consider an even E-region R. Note that any linear combination (with nonzero coefficients) of $\overline{p}(B, B')$, for $B' \in \mathcal{B}_R \backslash \{B\}$, must also violate rule (2.3) on at least one B'. Thus the linear combination is not in $Im(\Pi^0)$. In other words, the spanning set $\mathbb{D}_R$ is linearly independent on even E-regions and in this case $dim(\mathscr{D}_R) = \#B_R - 1$. A similar but less systematic conclusion has been drawn in [1] for triangular-quadrilateral hybrid meshes. Next, consider odd E-regions. From the previous analysis, we know that every even E-boundary component adds exactly one dimension to $\mathscr{D}_R$. Thus it suffices to study odd E-regions that contain only odd E-boundary components. Let R be such an E-region. We claim that the spanning set $\mathbb{D}_R$ is linearly dependent, but any $\#B_R - 2$ vectors in $\mathbb{D}_R$ are linearly independent. This can be proved by carefully connecting even paths into a chain (as shown in Figure 12(A)) and cutting through the chain, i.e., removing polygons on this chain, to get a simply connected E-region $\tilde{R}$. Note that $\tilde{R}$ can itself be viewed as a big even polygon. By Lemma 2.9, we have $dim(\mathcal{A}_{\tilde{R}}) = 1$. Pick a nonzero vector $\overline{c}^0 \in \mathcal{A}_{\tilde{R}} \subseteq C^0(\mathcal{K})$. It is not hard to see, as illustrated in Figure 12(A), that $\Pi^0(\overline{c}^0)$ is equal to a linear combination of $\overline{p}(*, *) \in \mathscr{D}_R$. Thus we have found a linear combination of $\mathbb{D}_R$ lying in $Im(\Pi^0)$ or, in other words, $\mathbb{D}_R$ is linearly dependent in $Ker(\Pi^1)/Im(\Pi^0)$. Finally, we shall show that any $\#B_R - 2$ vectors in $\mathbb{D}_R$ are linearly independent. Let $\overline{p}(B, \tilde{B})$ be the missing one in a $\#B_R - 2$ subset of $\mathbb{D}_R$. Similarly, we can make a cut through a chain of even paths, but the cut leaves $\tilde{B}$ untouched, as shown in Figure 12(B). This generates an odd E-region $\tilde{R}$ with two odd E-boundary components and $dim(\mathcal{A}_{\tilde{R}}) = 0$. Using linear algebra, induction, and the shifting of even paths, one can show that any nontrivial linear combination of the $\#B_R - 2$ vectors can not lie in $Im(\Pi^0)$ as this will eventually require a nonzero vector in $\mathcal{A}_{\tilde{R}}$, which does not exist. This completes the proof of the lemma. □

Proof of Lemma 2.13. With all the previous results and noting that obviously $\mathscr{D}_R \subseteq Ker(\Pi^1)/Im(\Pi^0)$ and the summation of $\mathscr{D}_R$ is a direct sum, the proof of Lemma 2.13 becomes simply a dimension counting. By Lemma 2.12 and equation (2.7),

Licensed to AMS.
License or copyright restrictions may apply to redistribution; see https://www.ams.org/journal-terms-of-use

one has

$$\begin{aligned} dim\left(\bigoplus_{R\in\mathcal{R}}\mathscr{D}_R\right) &= \sum_{R\in\mathcal{R}}(\#B_R-2)+\#R_e \\ &= -\sum_{R\in\mathcal{R}}\chi(R)+\#R_e \\ &= \sum_{R\in\mathcal{R}}(\#F_R-\#T_R-\#V_R)+\#R_e \\ &= \#F_e-\#T_e-\#V_e+\#R_e, \end{aligned}$$

which equals $nullity(\Pi^1)-rank(\Pi^0)$ according to Lemmas 2.10–2.11. □

Appendix B. Proof of lemmas in Section 2.4

Proof of Lemma 2.16. Since we already have Lemma 2.10, the proof of this lemma reduces to the proof of $\mathscr{A}_R\subseteq\tilde{C}_0^0(\mathcal{K})$. Note this is obviously true because the space $\mathscr{G}$ adds the missing alternating pattern on $\overline{\Gamma}_D$ back. The rank of Π_0^0 then follows from $dim(\tilde{C}_0^0(\mathcal{K}))=\#V_e^i+\sum_{B\in\mathcal{B}_e^b\cup\mathcal{B}^m}\eta(B)=\#V_e^i+\sum_{B\in\mathcal{B}}\eta(B)$. □

Proof of Lemma 2.19. The rank-nullity relation still works since we clearly have $\#F_e^i\geq\#T_e$ by induction. When $\#R^b=0$, i.e., each E-region contains at least one E-boundary component in $\mathcal{B}^i\cup\mathcal{B}^m$, the argument in the proof of Lemma 2.11 still works since any cluster of even polygons has "boundary" edges not on Γ_D. Thus we only need to consider the case $\#R^b=1$. Denote by R the only E-region in this case. There are two possibilities: R is odd or R is even. We first note that, similar to the proof of Lemma 2.11, one can show that any $\#T_e-1$ rows of Π_0^1 are linearly independent, i.e., $rank(\Pi_0^1)\geq\#T_e-1$. Consider the case when R is even. Let T_1 and T_2 be two even polygons in R. They can be glued together into a larger even polygon. The gluing process induces a linear combination of two rows of Π_0^1, corresponding to T_1 and T_2, respectively, into a new row representing the operation of Π_0^1 on the boundary of $T_1\cup T_2$. Repeat the gluing process until all polygons are glued together, as shown in Figure 13. We point out that this is possible since any "hole" inside an even E-region can be viewed just as an even polygon. Such an argument has already been used in the proof of Lemma 2.9. The gluing process

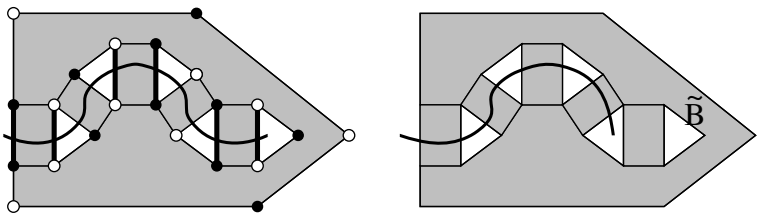

Figure 12. Cut through an odd E-region R with only odd E-boundary components. The solid curve marks the cut. In subfigure (A), a linear combination of $\overline{p}(*,*)\in\mathscr{D}_R$, shown in thick edge paths, is equal to $\Pi^0(\vec{c}^0)\in Im(\Pi^0)$, where $\vec{c}^0\in\mathcal{A}_{\tilde{R}}$ takes value $+1/-1$ on circled/solid vertices.

Licensed to AMS.
License or copyright restrictions may apply to redistribution; see https://www.ams.org/journal-terms-of-use

eventually leads to one giant even polygon with boundary $\partial R = \Gamma_D$, on which operator Π_0^1 is forced to be 0 because of the boundary condition. In other words, the gluing process generates a linear combination of the rows of Π_0^1 which is zero. Therefore in this case $rank(\Pi_0^1) = \#T_e - 1$. We can also see from the above analysis that the only possible way to generate a linear combination of the rows of Π_0^1 that vanishes on each column(edge) is by using the gluing process. When R is odd, note that the gluing process no longer works along odd E-boundary components, as illustrated in Figure 13. Thus in this case $rank(\Pi_0^1) = \#T_e$. Combining the above, this completes the proof of the lemma. □

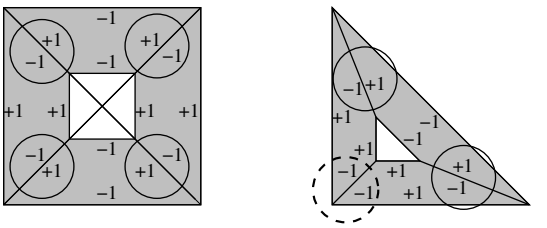

FIGURE 13. Gluing process. Inside each even polygon, assign alternating +1's and −1's to edges. When gluing two neighboring even polygons together into a larger polygon, one simply makes sure that the left and right values on each shared edge cancel with each other, as shown inside the solid circles. Such a gluing process works for even E-regions in the left graph, but not for odd E-regions in the right graph, since there will always be mismatched edges as shown in the dashed circle.

Proof of Lemma 2.20. The proof of this lemma is an extension of the proof of Lemma 2.12, as one shall use the same technique to analyze the linear independence relation in $Ker(\Pi_0^1)/Im(\Pi_0^0)$, which is omitted here in order to save space. It is obvious that $dim(\mathscr{D}_R) = 0$ for even $R \in \mathcal{R}^b$, since all E-boundary components are even and lie in $\mathcal{B}^b$. For even $R \notin \mathcal{R}^b$, the calculation of $dim(\mathscr{D}_R)$ is the same as in Lemma 2.12, except that $B \in \mathcal{B}_{e,R}^b$ are not counted. Finally, consider odd R. Note that odd E-boundary components alone contribute $\#B_{o,R} - 2$ to the dimension of $\mathscr{D}_R$, after replacing even paths by even loops when necessary. Then, by using degenerate even loops when necessary, each $B \in \mathcal{B}_{e,R}^i \cup \mathcal{B}_{e,R}^m$ contributes exactly 1 to the dimension of $\mathscr{D}_R$. This completes the proof of the lemma. □

Proof of Lemma 2.21. Since $\mathscr{D}_R \subseteq Ker(\Pi_0^1)/Im(\Pi_0^0)$, again the proof is just a dimension counting. Note the result of Lemma 2.20 can be rewritten as

$$dim(\mathscr{D}_R) = \begin{cases} (\#B_{o,R} + \#B_{e,R}^i + \#B_{e,R}^m - 2) + 2 & \text{for even } R \in \mathcal{R}^b, \\ (\#B_{o,R} + \#B_{e,R}^i + \#B_{e,R}^m - 2) + 1 & \text{for even } R \notin \mathcal{R}^b, \\ (\#B_{o,R} + \#B_{e,R}^i + \#B_{e,R}^m - 2) & \text{for odd } R. \end{cases}$$

Licensed to AMS.
License or copyright restrictions may apply to redistribution; see https://www.ams.org/journal-terms-of-use

Then one has

$$\begin{aligned} dim\left(\bigoplus_{R\in\mathcal{R}}\mathscr{D}_R\right) &= \sum_{R\in\mathcal{R}}(\#B_{o,R}+\#B^i_{e,R}+\#B^m_{e,R}-2)+\#R_e+\#R^b_e \\ &= -\sum_{R\in\mathcal{R}}(\chi(R)+\#B^b_{e,R})+\#R_e+\#R^b_e \\ &= -\sum_{R\in\mathcal{R}}\chi(R)-\#B^b_e+\#R_e+\#R^b_e \\ &= (\#F_e-\#T_e-\#V_e)-\sum_{B\in\mathcal{B}^b_e}\eta(B)+\#R_e+\#R^b_e \\ &= (\#F^i_e-\#T_e-\#V^i_e)-\sum_{B\in\mathcal{B}^m}\eta(B)-\sum_{B\in\mathcal{B}^b_e}\eta(B)+\#R_e+\#R^b_e \\ &= nullity(\Pi^1_0)-rank(\Pi^0_0). \end{aligned}$$

□

Acknowledgment

We thank Professor Jinchao Xu for valuable suggestions during the completion of this research work.

References

[1] R. Altmann and C. Carstensen, *P_1-nonconforming finite elements on triangulations into triangles and quadrilaterals*, SIAM J. Numer. Anal. **50** (2012), no. 2, 418–438. MR2914269

[2] B. Ayuso de Dios, K. Lipnikov, and G. Manzini, *The nonconforming virtual element method*, ESAIM Math. Model. Numer. Anal. **50** (2016), no. 3, 879–904. MR3507277

[3] L. Beirão da Veiga, F. Brezzi, A. Cangiani, G. Manzini, L. D. Marini, and A. Russo, *Basic principles of virtual element methods*, Math. Models Methods Appl. Sci. **23** (2013), no. 1, 199–214. MR2997471

[4] S. C. Brenner, *Forty years of the Crouzeix-Raviart element*, Numer. Methods Partial Differential Equations **31** (2015), no. 2, 367–396. MR3312124

[5] F. Brezzi, K. Lipnikov, and M. Shashkov, *Convergence of the mimetic finite difference method for diffusion problems on polyhedral meshes*, SIAM J. Numer. Anal. **43** (2005), no. 5, 1872–1896. MR2192322

[6] E. Brisson, *Representing geometric structures in d dimensions: topology and order*, Discrete Comput. Geom. **9** (1993), no. 4, 387–426. MR1206799

[7] Z. Cai, J. Douglas Jr., J. E. Santos, D. Sheen, and X. Ye, *Nonconforming quadrilateral finite elements: a correction*, Calcolo **37** (2000), no. 4, 253–254. MR1812789

[8] P. G. Ciarlet, *The Finite Element Method for Elliptic Problems*, Studies in Mathematics and its Applications, vol. 4, North-Holland Publishing Co., Amsterdam-New York-Oxford, 1978. MR0520174

[9] M. Crouzeix and P.-A. Raviart, *Conforming and nonconforming finite element methods for solving the stationary Stokes equations. I*, Rev. Française Automat. Informat. Recherche Opérationnelle Sér. Rouge **7** (1973), no. R-3, 33–75. MR0343661

[10] M. de Berg, M. van Kreveld, M. Overmars, and O. Schwarzkopf, *Computational Geometry: Algorithms and Applications*, Second, revised edition, Springer-Verlag, Berlin, 2000. MR1763734

[11] D. A. Di Pietro and A. Ern, *Discrete functional analysis tools for discontinuous Galerkin methods with application to the incompressible Navier-Stokes equations*, Math. Comp. **79** (2010), no. 271, 1303–1330. MR2629994

[12] D. A. Di Pietro, A. Ern, and S. Lemaire, *An arbitrary-order and compact-stencil discretization of diffusion on general meshes based on local reconstruction operators*, Comput. Methods Appl. Math. **14** (2014), no. 4, 461–472. MR3259024

Licensed to AMS.
License or copyright restrictions may apply to redistribution; see https://www.ams.org/journal-terms-of-use

[13] D. A. Di Pietro and S. Lemaire, *An extension of the Crouzeix-Raviart space to general meshes with application to quasi-incompressible linear elasticity and Stokes flow*, Math. Comp. **84** (2015), no. 291, 1–31. MR3266951
[14] J. Douglas Jr., J. E. Santos, D. Sheen, and X. Ye, *Nonconforming Galerkin methods based on quadrilateral elements for second order elliptic problems*, M2AN Math. Model. Numer. Anal. **33** (1999), no. 4, 747–770. MR1726483
[15] M. S. Floater, *Mean value coordinates*, Comput. Aided Geom. Design **20** (2003), no. 1, 19–27. MR1968304
[16] M. Floater, K. Hormann and G. Kós, *A general construction of barycentric coordinates over convex polygons*, Adv. Comp. Math. **24** (2006), 311–331.
[17] M. Floater, A. Gillette, and N. Sukumar, *Gradient bounds for Wachspress coordinates on polytopes*, SIAM J. Numer. Anal. **52** (2014), no. 1, 515–532. MR3166966
[18] M. S. Floater, *Generalized barycentric coordinates and applications*, Acta Numer. **24** (2015), 161–214. MR3349308
[19] A. Gillette, A. Rand, and C. Bajaj, *Error estimates for generalized barycentric interpolation*, Adv. Comput. Math. **37** (2012), no. 3, 417–439. MR2970859
[20] P. Gross and P. Kotiuga, *Data structures for geometric and topological aspects of finite element algorithms*, Progress in Electromagnetics Research **32** (2001), 151–169.
[21] H. D. Han, *Nonconforming elements in the mixed finite element method*, J. Comput. Math. **2** (1984), no. 3, 223–233. MR815417
[22] J. Hu and Z.-c. Shi, *Constrained quadrilateral nonconforming rotated $\mathcal{Q}_1$ element*, J. Comput. Math. **23** (2005), no. 6, 561–586. MR2190317
[23] J. Hu and S. Zhang, *Nonconforming finite element methods on quadrilateral meshes*, Sci. China Math. **56** (2013), no. 12, 2599–2614. MR3160068
[24] L. Kettner, *Using generic programming for designing a data structure for polyhedral surfaces*, Comput. Geom. Theo. Appl. **13** (1999), 65–90.
[25] I. Kim, Z. Luo, Z. Meng, H. Nam, C. Park, and D. Sheen, *A piecewise P_2-nonconforming quadrilateral finite element*, ESAIM Math. Model. Numer. Anal. **47** (2013), no. 3, 689–715. MR3056405
[26] L. C. Kinsey, *Topology of Surfaces*, Undergraduate Texts in Mathematics, Springer-Verlag, New York, 1993. MR1240053
[27] M. Köster, A. Ouazzi, F. Schieweck, S. Turek, and P. Zajac, *New robust nonconforming finite elements of higher order*, Appl. Numer. Math. **62** (2012), no. 3, 166–184. MR2878019
[28] H. Lee and D. Sheen, *A new quadratic nonconforming finite element on rectangles*, Numer. Methods Partial Differential Equations **22** (2006), no. 4, 954–970. MR2230281
[29] Y. Li, *A new family of nonconforming finite elements on quadrilaterals*, Comput. Math. Appl. **70** (2015), no. 4, 637–647. MR3372048
[30] Q. Lin, L. Tobiska, and A. Zhou, *Superconvergence and extrapolation of non-conforming low order finite elements applied to the Poisson equation*, IMA J. Numer. Anal. **25** (2005), no. 1, 160–181. MR2110239
[31] M. Mäntylä, *An Introduction to Solid Modeling*, Principles of Computer Science Series, vol. 13, Computer Science Press, Rockville, MD, 1988. MR918772
[32] M. Meyer, H. Lee, A. Barr and M. Desbrun, *Generalized barycentric coordinates for irregular polygons*, J. Graphics Tools **7** (2002), 13–22.
[33] L. Mu, X. Wang, and Y. Wang, *Shape regularity conditions for polygonal/polyhedral meshes, exemplified in a discontinuous Galerkin discretization*, Numer. Methods Partial Differential Equations **31** (2015), no. 1, 308–326. MR3285814
[34] J. R. Munkres, *Elements of Algebraic Topology*, Addison-Wesley Publishing Company, Menlo Park, CA, 1984. MR755006
[35] C. Park and D. Sheen, *P_1-nonconforming quadrilateral finite element methods for second-order elliptic problems*, SIAM J. Numer. Anal. **41** (2003), no. 2, 624–640. MR2004191
[36] R. Rannacher and S. Turek, *Simple nonconforming quadrilateral Stokes element*, Numer. Methods Partial Differential Equations **8** (1992), no. 2, 97–111. MR1148797
[37] E. H. Spanier, *Algebraic Topology*, McGraw-Hill Book Co., New York-Toronto, Ont.-London, 1966. MR0210112
[38] N. Sukumar and A. Tabarraei, *Conforming polygonal finite elements*, Internat. J. Numer. Methods Engrg. **61** (2004), no. 12, 2045–2066. MR2101599

Licensed to AMS.
License or copyright restrictions may apply to redistribution; see https://www.ams.org/journal-terms-of-use

[39] N. Sukumar and E. A. Malsch, *Recent advances in the construction of polygonal finite element interpolants*, Arch. Comput. Methods Engrg. **13** (2006), no. 1, 129–163. MR2283620
[40] E. L. Wachspress, *A Rational Finite Element Basis*, Mathematics in Science and Engineering, vol. 114, Academic Press, Inc. [A subsidiary of Harcourt Brace Jovanovich, Publishers], New York-London, 1975. MR0426460
[41] E. L. Wachspress, *Barycentric coordinates for polytopes*, Comput. Math. Appl. **61** (2011), no. 11, 3319–3321. MR2801997
[42] J. Wang and X. Ye, *A weak Galerkin mixed finite element method for second order elliptic problems*, Math. Comp. **83** (2014), no. 289, 2101–2126. MR3223326
[43] J. Warren, *Barycentric coordinates for convex polytopes*, Adv. Comput. Math. **6** (1996), no. 2, 97–108 (1997). MR1431788

School of Mathematical Sciences, Nanjing Normal University, Nanjing, People's Republic of China
Email address: yqwang@njnu.edu.cn

Licensed to AMS.
License or copyright restrictions may apply to redistribution; see https://www.ams.org/journal-terms-of-use